Physics and Chemistry of Minerals (2020) 47:51
https://doi.org/10.1007/s00269-020-01120-8

ORIGINAL PAPER

Short-range order and electronic structure of radiation-damaged zircon according to X-ray photoelectron spectroscopy

Yuliya V. Shchapova[1,2] · Dmitry A. Zamyatin[1,2] · Sergey L. Votyakov[1] · Ivan S. Zhidkov[2] · Andrey I. Kuharenko[2] · Seif O. Cholakh[2]

Received: 15 August 2020 / Accepted: 13 October 2020 / Published online: 4 November 2020

Abstract

Core-level and valence-band X-ray photoelectron spectroscopy was employed to study the dose-dependent radiation effects in the short-range order and the electronic structure of natural U, Th-bearing zircon near-surface layers. Single crystals from different localities (Ratanakiri, Cambodia; Mud Tank, Australia; Highlands, Sri Lanka) exhibiting wide variations in the accumulated radiation dose $D \approx (0 \div 9.2) \cdot 10^{18}$ α-decays/g was investigated. The dose values obtained by electron probe microanalysis and Raman micro-spectroscopy were used to correlate the samples with the two percolation transitions (p_1, p_2) in the amorphous-crystalline structure of damaged zircon. The dose-dependent variations in E_b (530.9–531.3, 101.7–102.4, 182.8- 183.3 eV) and FWHM (1.32–2.57, 1.47–1.77, 1.16 -1.55 eV) of the O1s, Si2p, and $Zr3d_{5/2}$ core levels, respectively, were attributed to changes in the ensemble of non-equivalent short-range order structures. An increase in the dose resulted in the complication of the oxygen sublattice, with the following nearest environments of O atoms: (1) O (Si, $^{[8]}$Zr, $^{[8]}$Zr), $E_b = 530.8$–531.2 eV, the amount of > ~3.5 apfu (at $D < p_1$); (2) O (Si, Si) and/or O (Si, Si, $^{[8]}$Zr), $E_b = 532.6$ eV, the amount of ~ $0.5 \div 0.8$ apfu (at $p_1 < D < p_2$); (3) O (Si, $^{[7]}$Zr, $^{[7]}$Zr), $E_b = 531.6$ eV, determined when the O (Si, $^{[8]}$Zr, $^{[8]}$Zr) amount is of ~ 1.7 apfu (at $D > p_2$). For the first time, under an increase in the radiation dose, the oppositely directed changes in the effective charges of Si and Zr cations were detected in damaged zircon. This phenomenon was assigned to an increase in the content of the short-range order fragments characteristic of pure oxides SiO_2 (namely, Si-O-Si) and ZrO_2 (namely, $^{[7]}$Zr) as well as to the influence of the anions O (Si, Si, $^{[8]}$Zr), and the assignment was independently confirmed by the valence band analysis. The sequence of transformations in the Si-O and Zr-O sublattices was shown to be not concurrent: a partial polymerization of SiO_4 tetrahedra occurs mainly at low and medium doses ($D < p_2$) both in the crystalline and amorphous fractions, while the 7-coordinated atoms $^{[7]}$Zr are mainly observed at higher doses ($D > p_2$) in the amorphous fraction.

Keywords Zircon · Radiation damage · Short-range order structure · XPES

Introduction

Zircon is a widespread accessory mineral that acts as a concentrator of lanthanides and actinides (Hoskin and Schaltegger 2003). In addition to its use in geochronometry and geothermobarometry due to its high chemical and physical resistance, zircon was also previously proposed as a material for the immobilisation of plutonium (Ewing et al. 1995). In the process of α-decay of U and Th impurities, natural zircon is subject to amorphisation under exposure to α-particles and recoil nuclei; here, the accumulated radiation dose D_α (the number of alpha events per gram of substance) depends on the concentration of radioactive impurities and the age of the sample (Murakami et al. 1991; Ewing et al. 2003). The presence of natural samples with variations of D_α from values close to zero to values sufficient for complete amorphisation makes zircon one of the most important model materials for studying radiation effects on a geological time scale.

At the level of long-range order, general regularities of structural degradation in zircon have been fairly well studied on the example of natural U- and Th-containing-,

✉ Yuliya V. Shchapova
shchapova@igg.uran.ru

[1] Zavaritsky Institute of Geology and Geochemistry of the Ural Branch of the Russian Academy of Sciences, Vonsovskii Str. 15, 620016 Yekaterinburg, Russia

[2] Institute of Physics and Technology of the Ural Federal University named after the first President of Russia B.N. Yeltsin, Mira Str. 19, 620002 Yekaterinburg, Russia

^{238}Pu-doped synthetic and ion-irradiated crystals [see, for example, the review and bibliography in (Ewing et al. 2003)]. In natural zircon, atomic displacements are caused by heavy recoil nuclei with an energy of ~ 70 keV, forming cascades of atomic displacements (~ 5000 atoms/recoil nucleus) and alpha particles with an energy of ~ 5 meV, which cause ionisation of atoms and the formation of point defects (~ 100 defects/α-particle) (Chakoumakos et al. 1987; Ewing et al. 1995; Salje et al. 1999; Ewing 2007; Farnan et al. 2007). On the basis of X-ray diffraction and transmission electron microscopy data [e.g., (Murakami et al. 1991; Weber et al. 1994; Rios et al. 2000)], it has been shown that radiation-induced degradation of zircon from crystalline to amorphous state can be described by two percolation transitions (Salje et al. 1999; Geisler et al. 2003; Trachenko et al. 2003; 2004). According to these studies, the structure of radiation-damaged zircon can be represented by two phases: crystalline (fraction f_c) and amorphous (f_a). In the region below the first transition (p_1), the crystalline phase prevails ($f_a < \sim 30\%$), while in the region above the second transition (p_2) the amorphous phase prevails ($f_a > \sim 70\%$); at the range from p_1 to p_2, the amorphous and crystalline phases coexist and mutually penetrate. For zircon samples obtained from Sri Lanka, the accumulated dose values of the first and second transitions are $\sim (2–3)\cdot 10^{18}$ and $\sim (4–5)\cdot 10^{18}$ α-decays/g, respectively (Salje et al. 1999; Ríos et al. 2000; Ewing et al. 2003). The dependence of the specific volume of the crystalline phase on the concentration of point defects and on the degree of expansion of the amorphous phase leads to tension–compression stresses of alternating signs in coexisting crystalline and amorphous regions (Salje et al. 1999; Ríos et al. 2000).

At the level of short-range order (SRO), the structure of crystalline and amorphous fractions remains controversial (see, for example, the review and bibliography in (Ewing et al. 2003; Nasdala et al. 2003)). The EXAFS method at T = 4.3 K has been used to show the shortening of the nearest interatomic distances < Zr-Zr > (from 3.64 Å to 3.34 Å), < Zr-O > (by 0.06 Å) and the decrease in coordination number of Zr from 8 to the average value of (6.8–7.2) ± 0.5) in metamict zircon compared to crystalline zircon; the data point out to the presence of baddeleyite-like edge-shared ZrO_7 polyhedra (Farges and Calas 1991; Farges 1994). A structural model suggested for aperiodic zircon annealed between 20 and 600° (Farges 1994) consists of angstrom-scale domains similar in SRO structure to simple oxides and zircon remnants, and three non-equivalent types of oxygen atoms are present in the structure. However, no evidence to Zr- and Si-rich domains of different coordination number was found in synthetic Pu-doped (Begg et al. 2000) and natural metamict (Barinsky, Kulikova 1977) zircon by the XAS method, and the amorphous state was suggested to retain the distorted, nearest-neighbor zircon SRO structure.

The MAS-NMR ^{29}Si method was applied to determine the chemical shift of silicon in metamict zircon; the data were interpreted as the presence of Si-O-Si bridging oxygen atoms in SiO_4 tetrahedra (Farnan 1999) (in contrast to regular three-coordinated O atoms (Si, $^{[8]}$Zr, $^{[8]}$Zr) in crystalline zircon). The broadening and small shift of the ^{29}Si peak at low-dose samples was associated with the disordering and the polymerisation of tetrahedra in crystalline regions; the appearance of a new wide peak of a higher chemical shift and its shift with increasing dose was related to increased polymerisation (Farnan and Salje 2001). The observations was interpreted in terms of the percolation model (Salje et al. 1999); a conclusion is drawn about the evolution of the structure of both crystalline and amorphous phases with increasing radiation dose (Trachenko et al. 2001).

The dose-dependent broadening and red shift of vibrational modes found by the Raman spectroscopy are interpreted as SRO degradation and expansion of the unit cell of the crystalline fraction in zircon (Nasdala et al. 1995, 1996, 2001; Wopenka et al. 1996; Pidgeon et al. 1998; Zhang et al. 2000b; Balan et al. 2001a; Geisler et al. 2001). Also the confinement effect may coarse band broadening due to phonon lifetime decrease in nano-crystallites [periodic domains of approximately < 5 nm in size at a dose of $> 1\cdot 10^{18}$ α-decays/g (Váczi and Nasdala 2017)] of highly damaged zircon (Geisler et al. 2001; Váczi and Nasdala 2017). In accordance with (Nasdala et al. 2001; Palenik et al. 2003), the width (FWHM) of the asymmetric stretching vibration mode B_{1g} of SiO_4 tetrahedra at ~ 1008 cm^{-1} is widely used as an empirical parameter of radiation dose. Partial preservation of short-range order in the amorphous fraction of damaged zircon was demonstrated by IR spectroscopy; the appearance of additional signals in the regions of 500–800 cm^{-1} and 1000–1300 cm^{-1} is attributed to Si–O–Si bonds arising during the polymerisation of silicon–oxygen tetrahedra in the amorphous and/or crystalline phase (Zhang et al. 2000a; Zhang and Salje 2001).

To develop the general understanding of the zircon metamictization process, it is important to establish the dependence of the ensemble of the SRO structures in amorphous and crystalline parts of zircon on the accumulated radiation dose, as well as to reveal the dose-dependent variations in the spectrum of electronic states generated by this ensemble of the SRO. Note that the data on electronic structure of damaged zircon are also necessary for interpreting the electronic spectra of optical absorption and luminescence, which are still partly controversial (Krasnobayev et al. 1988; Nasdala et al. 2003; Kempe et al. 2010, 2016; Votyakov et al. 2011).

Such information can be obtained by X-ray photoelectron spectroscopy (XPS), based on recording the energy spectrum of electrons knocked out from the surface layers of solid samples by X-ray radiation. The values of the binding

energy E_b of the electrons of the core levels and the valence band determined in this case depend on the short-range order structure, effective charge and characteristics of the chemical bonds in near-surface layers of solids (Siegbahn et al. 1974; Nefedov and Vovna 1987). A feature of the method is the thinness of the analysed layer, which is determined by the electron exit depth [< 10 nm (Siegbahn et al. 1974)]. However, by choosing the measurement conditions, photoelectrons from different depths can be detected (see, for example, reviews (Hochella 1988; Fadley, 2010)). It has been shown that, with X-ray excitation of AlK_α and a large photoelectron collection angle, ~ 90% of the measured intensity is provided by layers lying deeper than the surface monolayer (Nesbitt et al. 2014). When analysing appropriately prepared mineral surfaces (fresh cleavage), the information obtained can be correlated with their bulk properties (Zakaznova-Herzog et al. 2005, 2006). Another problem inherent to the XPS consists in the differential surface charge, which complicates the analysis of the shape of the spectral lines. In most cases the problem can be solved using spectrometers having an effective charge neutralisation system (Nesbitt et al. 2014).

In this work, the atomic and electronic SRO structure of Si, Zr polyhedra and the oxygen sublattice are studied using the XPS in a series of natural zircon samples with variations in the accumulated radiation dose from zero to close to a complete amorphisation dose. To quantify the radiation dose and the degree of damage in the samples, we use the data from electron probe microanalysis and Raman spectroscopy. Dose dependences of the binding energy of core levels of Si, Zr, and O and the width of the corresponding spectral lines, as well as the spectra of the valence band, are analysed taking into account the contributions of both the crystalline and amorphous fractions. On the base of the fitting of O1s superposition spectra by individual components related to variously coordinated oxygen atoms, the estimates of SiO_4—polymerisation degree are obtained. We show that the electronic structure of Zr-O and Si-O sublattices can be used to determine the sequence of their transformation in the metamictization process of zircon.

Samples

Single crystals of zircon from placer deposits of the Highlands of Sri Lanka (samples Z1-Z6), similar in properties to samples previously studied by X-ray diffraction, transmission electron microscopy, Raman and infrared spectroscopy, etc. (Murakami et al. 1991; Nasdala et al. 2004; Ginster et al. 2019), were studied. For comparison, we measured single crystals of highly crystalline zircon (called reference samples here) obtained in Ratanakiri, Cambodia from secondary deposits of alkaline basalt rocks after annealing at 1000 °C for 3 h (Zeug et al. 2018) (sample R1) and slightly damaged Mud Tank zircon from carbonatites in Australia (Black, Gulson 1978) (sample MT).

Methods

Electron probe microanalysis (EPMA) of chemical composition was performed according to the described method (Zamyatin et al. 2017). The errors in determining the matrix cations Zr and Si from a series of analyses (2σ) were 0.38 and 0.32 wt.%, respectively. After determining the content of the main and impurity elements at 15–29 points of each sample in two perpendicular directions passing through the centre of the crystal, the obtained data were averaged. The scatter of the elemental content values over the crystal surface was characterised by the value 2σ.

Raman spectra were measured on a Horiba LabRam HR800 Evolution spectrometer with 632.8 nm He-Ne laser excitation. Recording was carried out using a Czerny-Turner monochromator having a diffraction grating of 1800 grooves/mm by means of a multi-channel electrically-cooled silicon CCD detector with an operating range threshold frequency of ~ 900 nm. An Olympus BX-FM microscope was used with a 100X/NA = 0.9 lens and a controlled confocal aperture 100 μm; spatial resolution ~ 1 μm (lateral) and ~ 3 μm (depth); spectral resolution was ~ 1 cm^{-1}. When determining the true width of the Raman lines, a correction for spectral resolution was introduced according to (Váczi and Nasdala 2017). Spectra were recorded at 10–12 points for each crystal; after determining position ν and the width FWHM of the Raman mode B_{1g} at ~ 1008 cm^{-1} by approximating individual maxima in the spectra of Voigt contour, the obtained values were averaged. The scatter in the values of ν and FWHM over the crystal surface was characterised by 2σ.

XPS spectra were recorded on a high-resolution PHI XPS 5000 VersaProbe spectrometer (ULVAC-Physical Electronics, USA). The spectrometer has a classic X-ray optical scheme with a quartz monochromator; the operating range of the binding energy analyser is 0–1500 eV. The electrostatic focusing and magnetic shielding of the main camera supports high energy resolution (ΔE ≤ 0.5 eV for AlK_α excitation), spatial selectivity (minimum diameter of X-ray AlK_α probe d ~ 10 μm) and elemental sensitivity (up to a signal-to-noise ratio 10,000/3) for a wide range of objects. The spectrometer is fitted with a two-channel system for neutralising the electrostatic charge that arises during the registration of XPS spectra of dielectric samples. The neutralisation is carried out using both an electron source with a thermal cathode (~ 1 eV) and low-energy ions (≤ 200 eV). The spectrometer has an oil-free two-stage vacuum pumping system based on turbomolecular and magnetic discharge pumps providing a

working vacuum of ~ 10^{-7} Pa in the absence of contamination of samples with prevacuum oil vapours.

The measurements were carried out according to the previously developed methodology (Shchapova et al. 2020). The electron take-off angle of 90º corresponded to the maximum bulk sensitivity. The x-ray spot diameter was 100 µm. The X-ray radiation power on the sample did not exceed 25 W. In the survey spectra mode, the energy window width was 187.85 eV, while in the high-resolution mode in the region of the O1s, Si2p, Zr3d and C1s lines it was 23.5 eV. The measurements were carried out in vacuum with a residual pressure of argon ions ~ 1×10^{-6} Pa. The spectrometer energy scale was calibrated using the $Au4f_{7/2}$ and $Cu2p_{3/2}$ lines, while the effect of the width of the energy window on the FWHM was calibrated by the $Ag3d_{5/2}$ line. The initial processing of the spectra was carried out using the ULVAC-PHI MultiPak 9.8 software. Accounting for the sample charge was carried out according to the C1s level binding energy of 284.8 eV (Moulder et al. 1992). To reduce the contribution of the modified surface layers, the measurements were performed on a fresh crystal cleavage, after which the sample was immediately placed in the vacuum chamber of the spectrometer. The crystallographic orientation of the sample surface was not taken into account.

Results

Chemical composition, structural and chemical heterogeneity and degree of radiation damage according to EPMA and Raman microspectroscopy

The chemical compositions of the samples according to EPMA data are given in Table 1 along with the Raman spectra parameters. In Z1-Z6 samples, the content of basic Si, Zr, and O elements varies slightly over the crystal surface. The average content of impurity elements was: Hf—up to 1.876; U—up to 0.3591, Th—up to 0.1019 wt.%; other impurities—not more than 0.161 wt.%. The composition of the main elements taking Hf into account corresponds to stoichiometric amounts within 0.02 at.%. The content of radioactive elements increases in the series from Z1 to Z6. Relative variations in the uranium content are 6–17% in all samples except Z1, in which increased scatter (45%) is associated with a low content of U and, as a result, with a large relative error of measurements. The degree of chemical homogeneity of samples Z1-Z6 can be considered as satisfactory for the purposes of further analysis of XPS. In the reference samples R1 and MT, only the main elements and Hf are recorded by microprobe analysis; the content of other impurities is below the limit of determination (< 0.01 wt.%). According to LA-ICP-MS, the content of U and Th averages are 120 and 95 ppm, respectively, in sample R1 (Zeug et al. 2018), where the authors noted slight variations in the concentration of these elements. In the MT sample, the contents of U and Th are 6.2–56.5 and 2.0–40.1 ppm, respectively (our unpublished results); the obtained data are consistent with the U content of 6.1–36.5 ppm given in (Black and Gulson 1978). Unlike sample R1, the high scattering in the content of radioactive elements in sample MT indicates its chemical heterogeneity.

In the Raman spectra of samples Z1-Z6, the average values of Raman shift ν of the B_{1g} asymmetric stretching vibrations mode of SiO_4 tetrahedra shift from 1005.3 in Z1 to 995.3 cm^{-1} in Z5, while average FWHM values increase from 5.0 to 29.6 cm^{-1} (see Table 1); in sample Z6, the spectrum is broadened and mode B_{1g} is not distinguished. The relative scatter of the widths is 4% in sample Z1 and 10–13% in samples Z2-Z5; this allows us to consider their structural homogeneity as satisfactory for XPS analysis. In the reference sample R1, the average values of $\nu = 1008.0$ cm^{-1} and FWHM = 1.85 cm^{-1} are close to those in pure synthetic $ZrSiO_4$ crystals (Zeug et al. 2018). In sample MT, the average values of the parameters ν and FWHM are intermediate between R1 and Z1; the variation of the FWHM value within 15% is slightly higher than in samples Z1-Z6 and R1. That means the less homogeneous structure of MT, and is consistent with an increased heterogeneity in the radioactive impurity content.

The degree of radiation damage of the samples was quantified in two ways: (1) based on the calculation of the accumulated (time-integrated) dose of D_α in accordance with (Murakami et al. 1991; Ewing et al. 2003) taking the U and Th content and age of the samples [555 ± 11 Ma for Z1-Z6 (Nasdala et al. 2004); < 1 Ma for R1 (Zeug et al. 2018); 732 ± 5 million years for MT (Black and Gulson 1978)]; (2) based on calculating the equivalent dose D_α^{ed} in accordance with (Palenik et al. 2003; Váczi and Nasdala 2017) taking the FWHM width of the Raman mode at ~ 1008 cm^{-1}. Estimates obtained via the first method allow a comparison of our data with the results of earlier structural studies of Sri Lanka zircons presented in the literature, which used the same dose estimation method. The second method comprises an assessment of equivalent dose, i.e., the dose that samples with a given spectral line width would have had if there had been no thermal effects leading to the crystal structure recovering (Palenik et al. 2003). This method allows us to characterise the real degree of damage retained in the thermal history, and thus to compare data for zircon of different geneses.

The degree of radiation damage (see Table 1) varies from low in the Z1 sample ($D_\alpha = 0.62 \cdot 10^{18}$ α-decays/g, $D_\alpha^{ed} = 0.20 \cdot 10^{18}$ α-decays/g) to near total amorphization in Z5 ($D_\alpha = 5.58 \cdot 10^{18}$ α-decays/g, $D_\alpha^{ed} = 3.3 \cdot 10^{18}$ α-decays/g) and Z6 ($D_\alpha = 9.22 \cdot 10^{18}$ α-decays/g, D_α^{ed} not determined due to degradation of the Raman spectrum). To assess the

Table 1 Chemical composition according to electron probe microanalysis, position and FWHM of Raman mode B_{1g} near1008 cm^{-1} and the calculated values of accumulated radiation dose D_α and equivalent dose D_α^{ed} in samples R1, MT, and Z1-Z6

Sample	R1	MT	Z1	Z2	Z3	Z4	Z5	Z6
		Chemical composition [a] (2σ), wt.%						
Si		15.41 (0.16)	15.49 (0.26)	15.07 (0.38)	15.18 (0.39)	15.05 (0.33)	14.74 (0.38)	14.91 (1.04)
Zr		48.85 (0.84)	48.97 (0.33)	47.91 (0.47)	48.32 (0.34)	47.85 (0.27)	47.74 (0.41)	47.93 (0.60)
Hf		1.00 (0.02)	0.786 (0.017)	1.876 (0.042)	1.171 (0.021)	1.359 (0.071)	1.551 (0.026)	1.565 (0.032)
O		35.05	34.98	34.36	34.53	34.27	33.96	34.19
U	0.0119 (0.0068)[f]	n/d	0.0221 (0.0086)	0.0570 (0.0173)	0.0665 (0.0106)	0.1010 (0.0136)	0.2047 (0.0116)	0.3591 (0.0279)
Th	0.00942-0.00949[f]	n/d	0.0144 (0.0032)	0.0332 (0.0061)	0.0354 (0.0063)	0.1019 (0.0057)	0.0988 (0.0085)	0.0832 (0.0113)
Sum of other minor elements[b]		n/d	0.023	0.077	0.132	0.143	0.312	0.161
Total		100.34	100.29	99.39	99.45	98.88	98.61	99.20
Position[c] and FWHM[c] of B_{1g} Raman mode (2σ)								
Position, cm^{-1}	1008.0 (0.06)	1007.7 (0.30)	1005.3 (0.26)	1004.7 (0.34)	1001.0 (0.86)	998.3 (0.94)	995.3 (0.42)	-
FWHM, cm^{-1}	1.85 (0.36)	2.8 (0.36)	5.0 (0.18)	7.1 (0.92)	11.9 (1.3)	17.6 (1.8)	29.6 (3.8)	-
Accumulated radiation dose[d] D_α (2σ) and equivalent dose[e] D_α^{ed}(2σ)								
D_α, 10^{18}, α-decay/g	0.0004[f]	0.02 ÷ 0.22	0.62 (0.26)	1.59 (0.42)	1.84 (0.28)	3.09 (0.32)	5.58 (0.30)	9.22 (0.72)
D_α^{ed}, 10^{18}, α-decay/g	~0	0.06 (0.02)	0.19 (0.011)	0.33 (0.06)	0.68 (0.11)	1.22 (0.20)	3.42 (~1.0)	5.1 (>~1.0)

[a]Average values of the content of elements (at 15, 15, 19, 18, 29, 29 points in samples Z1, Z2, Z3, Z4, Z5, Z6, respectively); 2σ is the double standard deviation of the results from the average values obtained on each crystal (includes both analytical uncertainty and sample heterogeneity)

[b]Total content of impurity elements P, Ti, Fe, Y, Zr, Er, Tm, Yb, Pb; the content of Mg, Al, S, Ca, Mn, Fe, Y, Zr, Tb, Ho, Lu elements is below the detection limits (~0.01 wt.%) in all samples

[c]Average values for 10–12 points of each crystal; σ is the standard deviation of the results from the average values

[d]Average values of D_α (at 15, 15, 19, 18, 29, 29 points in samples Z1, Z2, Z3, Z4, Z5, Z6, respectively) calculated in accordance with (Murakami et al. 1991); σ is the standard deviation of the results from the average values

[e]Average values of D_α^{ed} (10–12 points of each crystal) calculated from the width of the $\nu_3(SiO_4)$ Raman mode B_{1g} in accordance with (Palenik et al. 2003; Váczi and Nasdala 2016):

$\nu_3(SiO_4)FWHM = A_1 - A_2\exp(-B_{FWHM}D_\alpha^{ed})$,

Where A_1 and A_2 are scaling factors ($A_1 = 34.96\ cm^{-1}$, $A_1 - A_2 = 1.8\ cm^{-1}$), $B_{FWHM} = 5.32\ 10^{-19}$ α-decay/g

[f] (Zeug et al. 2018)

actual degree of damage of the Z6 sample, we used a rough estimate using the "effective dose" $D_\alpha^{eff} = 0.55 \cdot D_\alpha$ (Nasdala et al. 2004), which approximately coincides with D_α^{ed}; for Z6, $D_\alpha^{eff} = 5.1 \cdot 10^{18}$ α-decays/g was obtained. The value of the accumulated dose $D_\alpha = 4 \cdot 10^{14}$ α-decays/g in sample R1 is significantly lower than ~$5 \cdot 10^{16}$ α-decays/g, which leads to spectrally detectable changes in the structure of zircon (Zeug et al. 2018). Since the width of the Raman mode B_{1g} in sample R1 coincides with that in pure synthetic $ZrSiO_4$ crystals, $D_\alpha^{ed} = 0$ can be obtained. For the MT sample, the degree of damage has intermediate values $D_\alpha = (0.02 \div 0.22) \cdot 10^{18}$ α-decays/g between R1 and Z1; a significant variation in the values of D_α is associated with distribution of radioactive elements. Assessment of the degree of damage by 10 points of analysis by Raman spectroscopy of the MT sample gave a lower value of $D_\alpha^{ed} \sim 0.1 \cdot 10^{18}$ α-decays/g.

Thus, Z1-Z6, R1 and MT samples cover virtually the entire range of the radiation damage degree in natural zircon. Within the framework of the percolation model (Salje et al. 1999; Rios et al. 2000), samples Z1, Z2, Z3 correspond to the first stage of damage (approximately, $f_a < 30\%$), Z4 to the second stage (approximately, $30\% < f_a < 70\%$), while Z5 and Z6 correspond to the third stage (approximately, $f_a > 70\%$). The samples R1 and MT can be considered as perfect crystalline zircon and a crystalline zircon having a low level of damage, respectively. The degree of chemical and structural homogeneity of the samples R1, Z1-Z6 is satisfactory for XPS analysis. In MT sample, the homogeneity is lower than in the others.

Core level and valence band X-ray photoelectron spectroscopy

Survey spectra

The survey spectra of Z1-Z6 samples are typical of zircon; the spectrum of sample Z1 is shown in Fig. 1. The electron binding energies are as follows: 525–535 eV (O1s), 425–445 (Zr 3s), 325–355 (Zr $3p_{3/2}$, $3p_{1/2}$), 275–290 (C1s), 176–190 (Zr $3d_{5/2}$, 3d $_{3/2}$), 145–160 (Si2s), 95–110 (unresolved Si $2p_{3/2}$, $2p_{1/2}$), < 60 eV (valence band Zr 4s, 4p, 4d; Si3s, 3p; O2s, 2p). These are close to those for crystalline zircon R1 (Shchapova et al. 2020); however, when recording in high resolution, they show differences (see below).

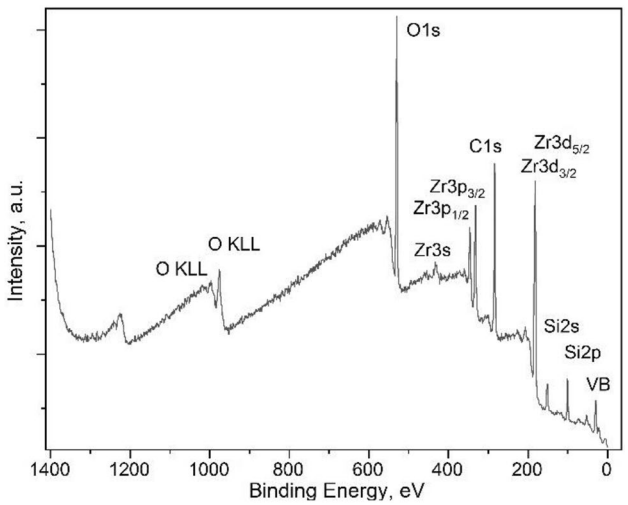

Fig. 1 Typical survey XPS spectrum of zircon from a series of samples from the central Highlands of Sri Lanka (sample Z1)

Core level spectra

The core level Si2p, Zr3d and O1s spectra of R1, MT and Z1-Z6 samples are shown in Fig. 2; the binding energies of O1s, Si2p, and $Zr3d_{5/2}$ are shown in Table 2.

The Si2p spectra (see Fig. 2a) represent an unresolved (splitting ~ 0.6 eV) spin–orbit doublet $Si2p_{3/2}$ and $Si2p_{1/2}$ (Moulder et al. 1992), forming a slightly asymmetrical peak. To determine the position (E_b) and width (FWHM) of the total Si2p peak, the spectra were approximated by one Voigt contour (Fig. 3a). Given the spectral resolution of the instrument (~ 0.5 eV), the one contour approximation seems reasonable; it was used before (Iacona et al. 1999; Balan et al. 2001b; Chanturia et al. 2017). The Si2p binding energy in R1 is E_b = 101.67 eV; this is close to the previously obtained values for crystalline zircon E_b = 101.8 eV [powder sample (Guittet et al. 2001)], 101.3 eV [green zircon from Mogok, Burma (Balan et al. 2001b)], 101.5 eV [sample from the Mir kimberlite pipe (Shchapova et al. 2010)], 102.1 eV [synthetic silicates $(ZrO_2)_x(SiO_2)_{1-x}$ at x = 0.52 (Lucovsky 2006)]. The FWHM of Si2p peak in sample R1 is 1.47 eV.

In the series R1, MT, Z1-Z5, the simultaneous growth of E_b (from 101.67 to 102.42 eV) and FWHM (from 1.47 to 1.77 eV) Si2p is observed; in Z6, a slight decrease in the values of E_b and FWHM was obtained (see Table 2).

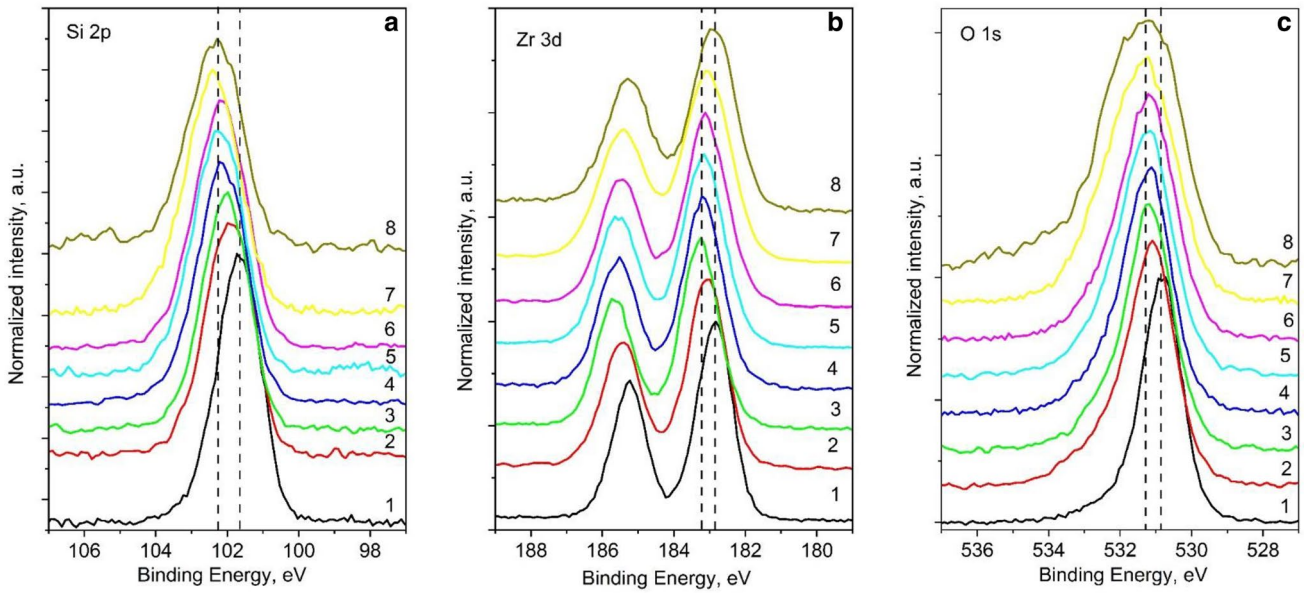

Fig. 2 Spectra of Si2p (**a**), Zr3d (**b**), O1s (**c**) of zircon samples R1 (1), MT (2) and Z1-Z6 (3–8, respectively). Dased lines represent the range of variations in the positions of the maxima. Spectra are spaced on an intensity scale for clarity

Table 2 Binding energy E_b and the linewidth FWHM of the O1s, Si2p, $Zr3d_{5/2}$ spectra in samples R1, MT, and Z1-Z6

Sample	O1s [a]			Si2p (3/2 and 1/2)		$Zr3d_{5/2}$	
	E_b, eV	FWHM ($O_1$1s), eV	FWHM ($O_2$1s), eV	E_b, eV	FWHM, eV	E_b, eV	FWHM, eV
R1	530.9	1.27 (0.01)	1.83 (0.16)	101.67 (0.01)	1.47 (0.02)	182.84 (0.008)	1.16 (0.02)
MT	531.1	1.50 (0.01)	1.78 (0.10)	101.95 (0.01)	1.59 (0.02)	183.07 (0.004)	1.26 (0.01)
Z1	531.2	1.52 (0.02)	1.02 (0.16)	102.05 (0.01)	1.54 (0.02)	183.27 (0.004)	1.25 (0.01)
Z2	531.1	1.51 (0.02)	1.54 (0.10)	102.15 (0.01)	1.64 (0.02)	183.19 (0.006)	1.31 (0.02)
Z3	531.2	1.64 (0.02)	1.66 (0.10)	102.25 (0.01)	1.68 (0.02)	183.18 (0.004)	1.41 (0.01)
Z4	531.2	1.71 (0.02)	1.48 (0.14)	102.20 (0.01)	1.73 (0.02)	183.10 (0.006)	1.41 (0.02)
Z5	531.3	1.92 (0.02)	1.81 (0.10)	102.42 (0.01)	1.77 (0.02)	183.06 (0.004)	1.55 (0.01)
Z6	531.3	2.09 (0.24)	2.57 (0.32) (E_b = 531.6) 4.40 (0.9) (E_b = 532.8)	102.35 (0.02)	1.75 (0.04)	182.87 (0.006)	1.41 (0.01)

[a]The value of E_b (O1s) corresponds to the spectral maximum obtained to a first approximation by fitting the O1s spectrum by one general Voigt contour. The values of FWHM ($O_1$1s) and FWHM ($O_2$1s) are obtained by fitting the O1s spectrum by two Voigt contours with fixed maximum values 531.2–532.6 eV for samples Z1-Z5, 530.8–532.0 eV for samples R1, MT; the spectrum of the Z6 sample is approximated by decomposing into three Voigt components. Uncertainties (2σ) of the values of E_b and FWHM characterise the signal-to-noise ratio and the quality of the spectra fitting

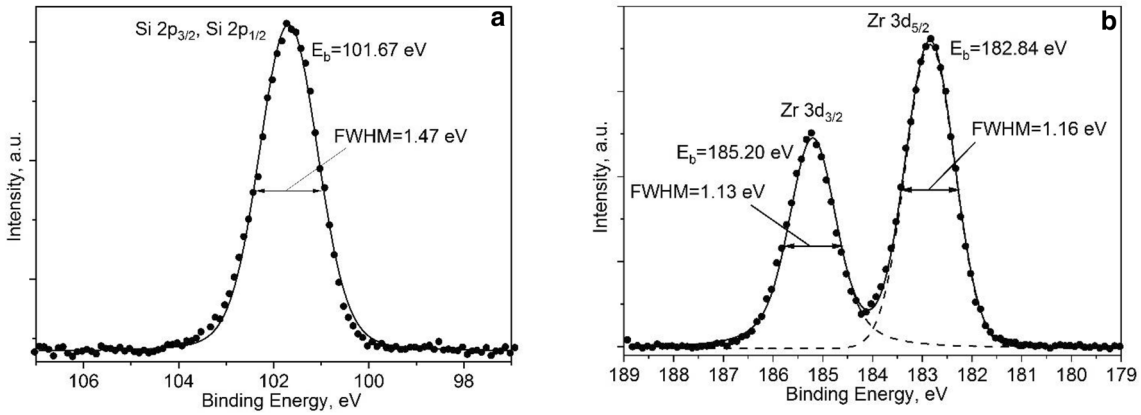

Fig. 3 Determination of the E_b and FWHM parameters of Si2p (**a**) and Zr3d (**b**) spectra of zircon (filled circles) based on the approximation by the Voigt contour (solid and dashed lines) after subtracting Shirley background (sample R1)

Spectra Zr3d of samples Z1-Z6 are represented by two lines from the well-resolved components of the spin–orbit splitting $Zr3d_{5/2}$ and $Zr3d_{3/2}$ (see Fig. 2b). The binding energies are determined by approximating the Zr3d spectrum by two Voigt contour (Fig. 3b). The value of E_b = 182.84 eV of the component $Zr3d_{5/2}$ in zircon R1 is close to the previously obtained 182.95 eV [powder sample (Guittet et al. 2001)], 182.7 eV [zircon from the Mir kimberlite pipe (Shchapova et al. 2010)], 182.6 eV [green zircon from Mogok, Burma (Balan et al. 2001b)], 182.65 eV [synthetic silicates $(ZrO)_x(SiO)_{1-x}$ at x = 0.52 (Lucovsky 2006)]. In the samples MT and Z1, the value of E_b increases to 183.07 eV and 183.27 eV. In the series of samples Z1-Z6, the value of E_b successively decreases from 183.27 in Z1 to 182.87 eV in Z6. The FWHM grows from 1.25 eV to 1.55 eV (see Table 2). The shape of the broadened lines of Z5 and Z6 samples is distorted, and their non-elementary nature can be suggested; but unambiguous deconvolution of the spectrum is difficult.

Thus, the trend in the binding energy $Zr3d_{5/2}$ (increase in E_b with an increase in the degree of damage) coincides with that for Si2p in only three samples R1-MT-Z1; in the samples of the Z1-Z6 series, the trend has the opposite direction. Due to the distorted shape of the $Zr3d_{5/2}$ spectra of samples Z5 and Z6, it is possible that they are not elementary. In sample Z6, a slight narrowing of the Zr3d line was observed, similar to that for the Si2p line.

Spectra O1s of R1, MT, and Z1-Z6 samples are represented by an asymmetric line having a "wing" in the high-energy part. The fitting of the entire profile of the samples to a first approximation by one general Voigt contour gives values of 530.86 ÷ 531.3 eV (see Table 2), but does not

reproduce the shape of the lines accurately. The estimated energies are close to the previously obtained values of 530.95 eV [sample from the Mir kimberlite pipe (Shchapova et al. 2010)], 530.6 eV [green zircon from Mogok, Burma (Balan et al. 2001b)], 531.3 eV (powder sample, (Guittet et al. 2001)), 531.4 eV [synthetic silicates $(ZrO)_x(SiO)_{1-x}$ at $x = 0.52$ (Lucovsky 2006)]. As with other core levels, the discrepancies of E_b(O1s) in the literature can be partially explained by small differences in the reference C1s binding energy (Greczynski and Hultman 2018), as well as by charge or structural effects. The FWHM = 1.32 eV of the entire O1s contour in the R1 sample is close to the lowest values of FWHM ~ 1.3 eV measured in crystalline silicates at $T = 300$ K by spectrometers with the spectral resolution ~ 0.35 eV and the high efficiency of charge neutralization system; this value is characteristic of silicates with single structural type of oxygen atom, such as quartz and olivine (Nesbitt et al. 2014; Zakaznova-Herzog et al. 2005, 2006; Bancroft et al. 2009). This makes it possible to relate further the variations in shape and width of the spectra of damaged zircon samples to the transformation of their structure.

An accurate analysis of the line shape of sample R1 using the fitting over the low-energy part (Fig. 4a) showed that the O1s line can be represented by two maxima: the main $E_b(O_1 1s) = 530.8$ eV and the additional $E_b(O_2 1s) = 532.1$ eV (with the relative intensity ~ 8%). The obtained E_b values were used to fit the spectrum of the MT sample (see Table 2). Low-energy part fitting of the O1s line of Z1 sample gives slightly higher values of $E_b(O_1 1s) = 531.2$ eV and $E_b(O_2 1s) = 532.6$ eV (Fig. 4b); these were used to fit the spectra of Z2-Z6 samples (Fig. 5). The dominant component $O_1 1s$ corresponds to the three-coordinated oxygen O_1(Si, $^{[8]}$Zr, $^{[8]}$Zr) (Guittet et al. 2001), while the component $O_2 1s$ is not typical for zircon spectrum. A gradual increase in the relative area of $O_2 1s$ component is observed from 8% (in Z1) to 30% (in Z5), as well as an increase in its width (see Table 2). For sample Z6, it is not possible to fit the spectrum by two contours; therefore, the third contour was introduced, and the $E_b = 531.6$ eV of an additional component was obtained; the total contribution of the second and the third components is > 50% (see Fig. 5f).

Thus, the spectra of core levels of Si2p, Zr3d and O1s demonstrate regular changes in position, width and shape in the series of samples R1, MT1, Z1-Z6. The position of the maxima shifts towards high binding energies in the spectrum of Si2p and O1s and shows a nonmonotonic behaviour in the spectrum of Zr3d. The width of all lines increases (with few exceptions). Two non-equivalent states $O_1 1s$ and $O_2 1s$ are observed, the first of which corresponds to the three-coordinated oxygen atom in zircon O_1(Si, $^{[8]}$Zr, $^{[8]}$Zr). The proportion of the second increases in the series of samples R1, MT1, Z1-Z6. An additional (third) contribution with $E_b = 531.6$ eV was observed in Z6 sample.

Valence band (VB) spectra

The valence band spectra (Fig. 6) show O2p- (5–10 eV), O2s- (22–25 eV) and Zr4p- (30–33 eV) subbands (Rignanese et al. 2001; Shchapova et al. 2010; Du et al. 2012). In addition, a subband is recorded in the region of 17–19 eV, which is probably associated with uncontrolled surface carbon [see, for example, (Haensel et al. 2012)]. In the series of samples R1, MT1, Z1-Z6, a change in the relative

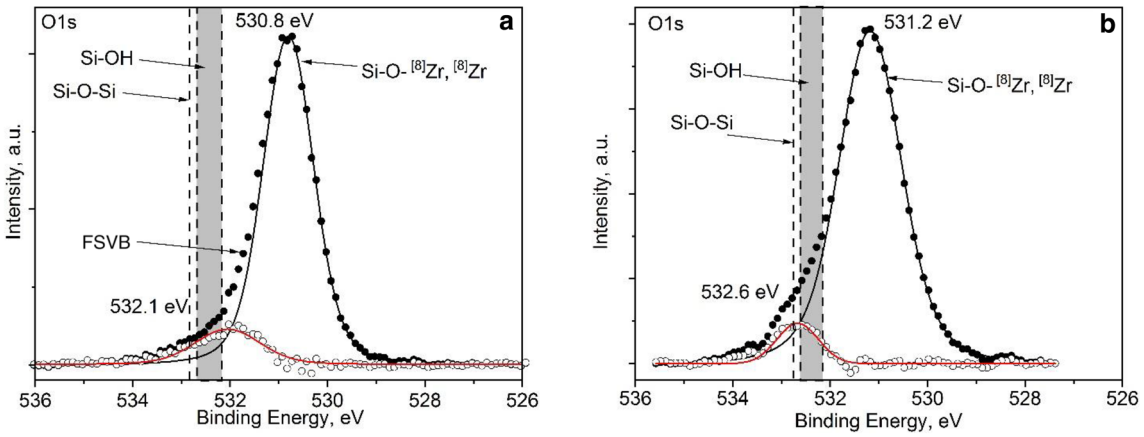

Fig. 4 Analysis of the O1s line shape of samples R1 (**a**) and Z1 (**b**) after subtracting Shirley background, showing the non-elementary nature of the spectra and the dissimilarity in their high-energy parts. Filled circles—experiment, black solid lines—approximation of the low-energy part of the spectra by the Voigt profile, unfilled circles—difference between the experimental and fitted spectra, red solid lines—approximation of the difference spectra by the Voigt profile. Vertical dashed lines mark values of the binding energy of oxygen atoms in silicates in the coordination of Si–OH (Duval et al. 2002; Zakaznova-Herzog et al. 2008) and Si–O-Si (Guittet et al. 2001; Zakaznova-Herzog et al. 2005); the possible contribution of FSVB effect (Bancroft et al. 2009) is also shown

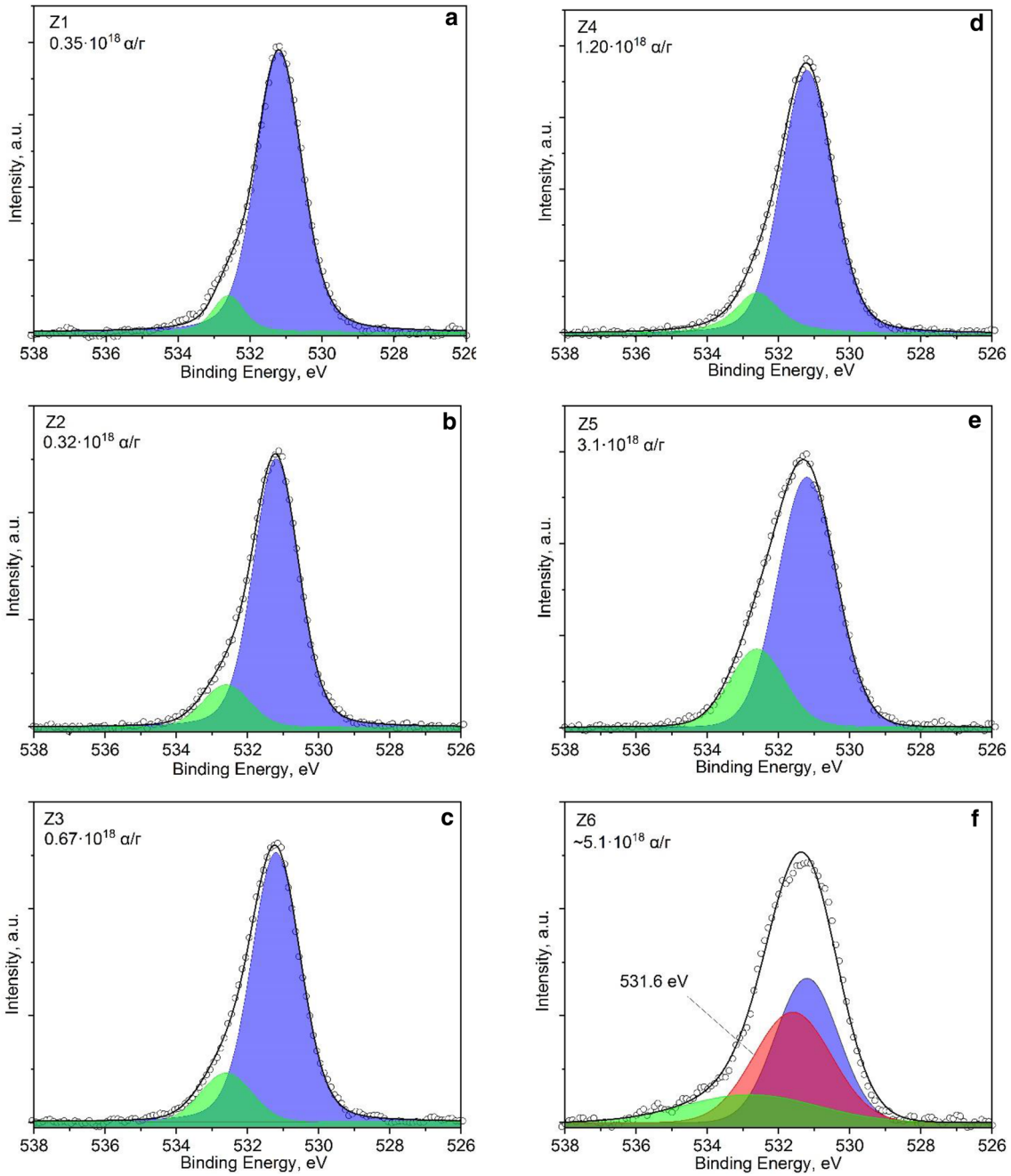

Fig. 5 Evolution of the O1s spectrum of zircon samples Z1-Z6 (a-f, respectively) with an increase in the equivalent dose of D_{α}^{ed} (values of D_{α}^{ed} are shown in the figures): experimental data (unfilled circles), fitting of the spectra by two Voigt contours with fixed maxima position of 531.2 eV (blue) and 532.2 eV (green); total spectrum (black line). To satisfactorily fit the spectrum of sample Z6, an additional Voigt contour (red) with a maximum of 531.6 eV is introduced

intensity of the peaks of the O2p subband is recorded. A decrease in the relative intensity of deep binding states at ~ 10.7 and ~ 8.9 eV is observed along with the appearance of an additional peak of ~ 13 eV. The form of the O2s subband changes slightly, and the position of the Zr4p subband varies across the range 30.8–31.8 eV.

Discussion

FWHM dose dependences

It is known that the width of the XPS spectral line of

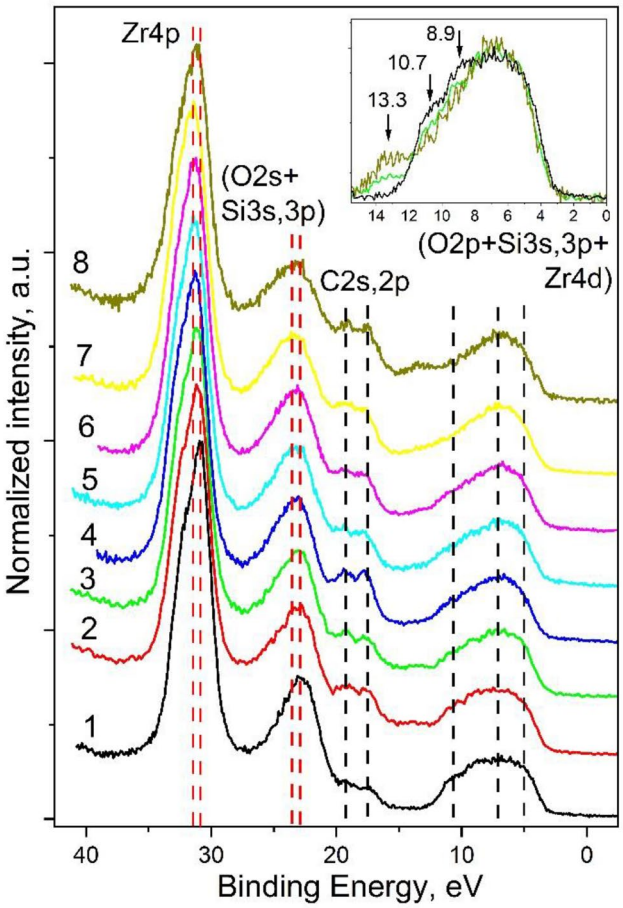

Fig. 6 Valence band spectra of zircon samples R1 (1), MT (2) and Z1-Z6 (3–8, respectively), and the nature of the main subbands according to calculations [Rignanese et al. 2001; Shchapova et al. 2010] (for $ZrSiO_4$) and [Haensel et al. 2012] (for C). The black dashed lines mark the position of the maxima in the experimental spectra of the O2p and C2p subbands; the red dashed lines show the range of variations in the position of the maxima of the O2s and Zr4p subbands. Spectra are spaced on an intensity scale for clarity. The inset shows the O2p subband of samples R1, Z1 and Z6 as an example, indicating their differences in the density of O2p states

dielectrics is determined by a number of effects: (1) variations in the chemical shift of elements due to non-equivalent structures of short-range order and different charge states of atoms; (2) differential surface charge and instrumental broadening; (3) phonon broadening, i.e., a decrease in the excited state lifetime with temperature due to interaction with phonons; (4) final state vibrational broadening/splitting (FSVB/FSVS); (5) the possible contribution of surface states; (6) variations in the work function of electrons with differences in band bending on the surface [see, for example, (Bancroft et al. 2009; Nesbitt et al. 2014)]. Since in crystalline zircon $ZrSiO_4$ (space group $I4_1/amd$) all oxygen, silicon and zirconium atoms are crystallographically equivalent (Finch and Hanchar, 2003), the effect (1) must be zero in the highly crystalline R1 sample. The FWHM values obtained for O1s and Si2p of sample R1 are close to their lowest measured values ~ 1.3 eV in silicates (quartz, olivine) at $T = 300$ K by spectrometers with the spectral resolution ~ 0.35 eV and the high efficiency of charge neutralization system (Zakaznova-Herzog et al. 2005, 2006; Bancroft et al. 2009; Nesbitt et al. 2014). Thus, the effect (2) of the differential charge of the surface can be considered insignificant with the used measurement procedure as compared with the temperature symmetric line broadening associated with phonon states population, the effect (3). The slight asymmetry of the O1s and Si2p spectra for zircon R1 can be caused by the effect (4) of FSVB (Bancroft et al. 2009). In addition, the asymmetry may be associated with slight surface hydroxylation after cleavage with the appearance of surface species Si–OH [E_b (O1s) = 532.2–532.7 eV (Duval et al. 2002; Zakaznova-Herzog et al. 2008)]. No other effects (5) of surface states contribution were detected. The effect (6) of the electron work function variations is generally considered to be negligible [< 0.1 eV (Chambers et al. 2009; Bancroft et al. 2009)].

With these considerations in mind, we ascribed the increase in FWHM of Si2p, Zr3d, $O_1$1s and $O_2$1s spectra at the increasing radiation dose (Fig. 7, Table 2) to the effect (1), namely the growth in the variety of SRO structures (i.e., disordering) followed by the dispersion of the chemical shift of the core levels. It can be caused by changes in the SRO of the crystalline or amorphous phases, or both phases simultaneously. The small contribution of surface OH groups to the FWHM broadening is also possible; other effects can be ignored in the first approximation.

The dependences of FWHM on the equivalent dose D_α^{ed} are fitted by the dose function (see Fig. 7):

$$P = A_1 - A_2 \exp(-BD_\alpha^{ed}) \quad (1)$$

where P is a structurally sensitive parameter—in this case, FWHM. The fitting parameters A_1, A_2 and B means the follows: A_1—FWHM value at the highest chemical shift dispersion (disordered state); difference (A_1-A_2)—FWHM value at the initial (ordered) state; B – cross section of the disordering process.

The fitting parameters (Table 3) show that disordered state corresponds to the FWHM values of 1.77, 1.51 and 1.95 eV for Si2p, Zr3d and $O_1$1s, respectively. Cross section B was obtained maximally for the Si2p line width, somewhat lower for Zr3d and minimally for $O_1$1s. It means that the most effective broadening of the electronic state spectra occurs: at low doses ($D_\alpha^{ed} \sim p_1$) for Si2p; at higher doses (up to $p_1 < D_\alpha^{ed} < p_2$) for Zr3d (see Fig. 7); at virtually the entire range of doses (up to $D_\alpha^{ed} > p_2$) for $O_1$1s. Therefore, most of the possible types of SRO in the silicon-oxygen

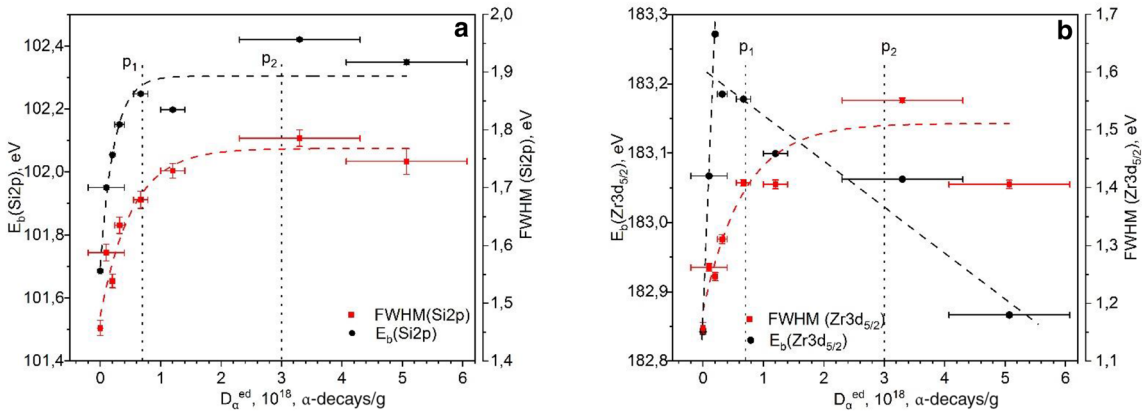

Fig. 7 Dose (D_α^{ed}) dependences of E_b (black symbols) and FWHM (red symbols) values of Si2p (**a**) and Zr3d (**b**) spectra of zircon samples R1, MT and Z1-Z6. Symbols—experiment; dashed lines—approximation by dose response function (or linear function for $Zr3d_{5/2}$). The dotted lines mark D_α^{ed} values that approximately correspond to p_1 and p_2 percolation points

Table 3 Fitting parameters of dose dependences of the spectral characteristics (E_b and FWHM) for Si2p, $Zr3d_{5/2}$ and $O_1$1s spectra

Spectrum	Spectral characteristic	Fitting parameters			
		A_1 (σ), eV	A_2(σ), eV	B, 10^{-18}, (α-decays/g)$^{-1}$	Adj.R^2
Si2p	E_b	102.3 (0.04)	0.60 (0.08)	4.4 (1.3)	0.8948
Si2p	FWHM	1.77 (0.03)	0.28 (0.03)	1.9 (0.6)	0.9010
$Zr3d_{5/2}$	FWHM	1.51 (0.03)	0.32 (0.06)	1.5 (0.7)	0.8088
$O_1$1s	FWHM	1.95 (0.13)	0.6 (0.13)	0.96 (0.46)	0.8412

sublattice are formed at $f_a < 30\%$, and in the zirconium-oxygen at $f_a < 70\%$, i.e., it is associated with both crystalline and increasing amorphous fraction. The change in the SRO of oxygen atoms also continues at $f_a > 70\%$, indicating possible changes in the structure of the amorphous fraction at high doses. Thus, radiation disordering of the Si- and Zr-sublattices does not occur simultaneously; it is probably associated with different phases: for Si, both with the crystalline and amorphous phase; for Zr, primarily with amorphous phase. A decrease in dispersion of Si2p and Zr3d chemical shift in the Z6 sample may be attributed to the predominance of certain SRO types in the amorphous sample, which is consistent with the distortion of the Zr3d line shape in this sample and the appearance of an additional type of oxygen in the O1s spectrum.

Dose dependences of non-equivalent oxygen atom concentration

Dose dependences of the concentration of oxygen atoms were calculated as areas S_1 and S_2 of the $O_1$1s and $O_2$1s contours with normalisation to 4 atoms per formula unit (apfu) (Fig. 8). In Z1-Z4 samples ($D_\alpha^{ed} < p_1$ in Z1-Z3 and $p_1 < D_\alpha^{ed} < p_2$ in Z4) the concentration of O_2 is $S_2 = 0.3$–0.6 apfu and increases slowly, whereas in samples Z5, Z6 ($D_\alpha^{ed} > p_2$) it is $S_2 = 0.9$–2.3 apfu and increases rapidly with increasing dose.

The binding energy $O_1$1s (530.8 in R1, MT and 531.2 eV in Z1-Z6) corresponds to the main type of oxygen atoms in zircon O (Si, $^{[8]}$Zr, $^{[8]}$Zr) (see Sect. 2.2). The binding energy $E_b(O_2 1s) = 532.6$ eV for samples Z1-Z6 is close to E_b of the oxygen atoms in coordination of Si–O-Si in quartz [532.6 eV (Zakaznova-Herzog et al. 2005), 532.7 eV (Guittet et al. 2001)] and quartz glass [533.18 eV (Nesbitt et al. 2014)]. Therefore, the contribution of $O_2$1s in the Z1-Z6 samples is assigned to the oxygen O (Si, Si) of partially polymerised tetrahedra with Si-O-Si bridges. The result obtained agrees with the conclusion about partial polymerization of SiO_4 tetrahedra in radiation-damaged zircon according to MAS-NMR ^{29}Si and IR spectroscopy (Farnan 1999; Farnan and Salje 2001; Zhang et al. 2000a; Zhang and Salje 2001). Also, the appearance of chains of connected SiO_n polyhedra in the damaged structure was established by the molecular dynamics modelling (Trachenko et al. 2001). The formation of Si-O-Si fragments in crystalline zircon during structural relaxation (1) near oxygen divacancies and (2) near oxygen vacancies stabilised by zirconium vacancies was previously established in our semi-empirical structural modelling (Votyakov et al. 2011). The nearest environment of oxygen atom in these distorted fragments was predicted

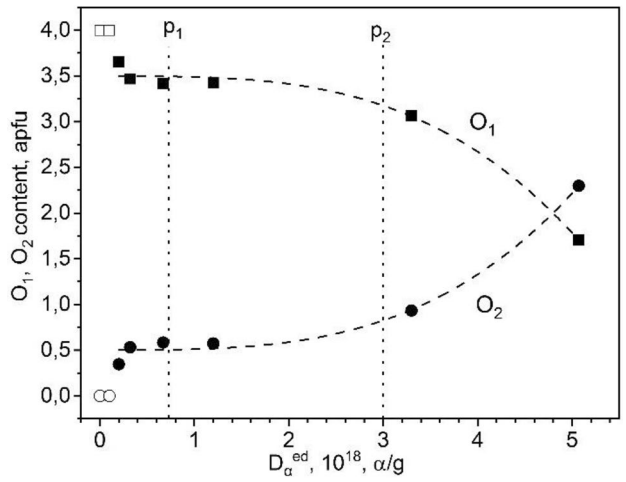

Fig. 8 Dose (D_α^{ed}) dependences of the concentration of non-equivalent oxygen atoms O_1 (filled squares) and O_2 (filled circles), determined by the area of the $O_1$1s and $O_2$1s contours with E_b = 531.2 and 532.6 eV for samples Z1-Z6 (accounting an additional contribution at 531.6 for sample Z6), normalised to 4 atoms O. For samples R1 and MT (unfilled simbols), the contribution of $O_2$1s with E_b = 532.6 eV is taken as equal to zero. The dotted lines mark D_α^{ed} values that approximately correspond to p_1 and p_2 percolation points

to consist of two silicon atoms and one zirconium atom O (Si, Si, [8]Zr). According to the *ab initio* quantum-chemical calculation, the effective charge of this oxygen atom does not differ significantly from O (Si, Si) (Votyakov et al. 2011). In contrast to samples Z1-Z6, the E_b = 532.1 eV of a small (< 10%) contribution of $O_2$1s in R1 and MT samples corresponds well to E_b value of the surface oxygen atoms in coordination of Si-OH [E_b = 532.2–532.7 eV (Duval et al. 2002; Zakaznova-Herzog et al. 2008)], as well as it can be assigned to FSVB effect (Bancroft et al. 2009). Thus, for samples R1 and MT, the concentration of O_2 atoms is taken as equal to zero (see Fig. 8).

It can be assumed that the slow increase in concentration of O (Si, Si) and/or O (Si, Si, [8]Zr) atoms at $D_\alpha^{ed} < p_1$ is partly secured by the vacancy defects accumulation in crystalline fraction; this possibility was not excluded in (Farnan 1999; Farnan and Salje 2001). However, the low concentration of oxygen vacancies ~ (1–7)·10^{20} cm^{-3} in Z1-Z4 samples [estimated by D_α^{ed} taking into account the number of vacancies formed by one alpha particle according to (Votyakov et al. 2011)] is hardly sufficient for the concentration of O_2 atoms observed; therefore, the contribution of the growing amorphous fraction should be taken into account as well.

At $D_\alpha^{ed} > p_2$, the rapid growth of O (Si, Si) and/or O (Si, Si, [8]Zr) is obviously ensured by the dominant amorphous fraction. The appearance of an additional (third) type of oxygen with E_b ~ 531.6 eV in Z6 indicates some changes in the SRO structure of the amorphous phase at $D_\alpha^{ed} > p_2$. The binding energy of this type of oxygen is of intermediate value between the E_b of $O_1$1s and $O_2$1s. An increase in the E_b(O1s) from 531.2 eV for O (Si, [8]Zr, [8]Zr) to ~ 531.6 eV can be provided by a decrease in the coordination number of the neighboring Zr atoms from 8 to ~ 7 because of the chemical bond [7]Zr-O is suggested to be less ionic than [8]Zr-O. Previously, the presence of ZrO_7 polyhedra in metamict zircon was observed by EXAFS (Farges and Calas 1991; Farges 1994). It can be assumed that E_b ~ 531.6 eV corresponds to O (Si, [7]Zr, [7]Zr), which is in accordance with "bond length—bond strength" model constructed in (Farges 1994) on the base of EXAFS data. No contribution of oxygen atoms characteristic of monoclinic ZrO_2 (E_b ~ 530.0 eV), were found.

Note that the observed S_1/S_2 ratio can be provided by various sets of silicon-oxygen tetrahedra Q_n (n = 0–4, where n is the number of bridging oxygen atoms). An increase in the diversity of Q_n should lead to increase in variations in the chemical shift of oxygen; this fact apparently brings the broadening of the lines $O_1$1s and $O_2$1s with increasing dose.

Thus, a complication of the oxygen sublattice structure with increasing dose is observed in Z1-Z6 zircons. The following SRO structures of oxygen atoms were distinguished: (1) three-coordinated oxygen O (Si, [8]Zr, [8]Zr) with E_b = 531.2 eV which is characteristic of crystalline zircon and is the main type of oxygen at $D < p_1$; (2) radiation damage-induced atoms O (Si, Si) and/or O (Si, Si, [8]Zr) with E_b = 532.6 eV, the concentration of which increases slowly at the range from D_α^{ed} ~ p_1 to D_α^{ed} ~ p_2; (3) an additional type of oxygen with E_b ~ 531.6 eV, well-determined in heavily-damaged zircons at $D_\alpha^{ed} > p_2$ and presumably associated with the oxygen O (Si, [7]Zr, [7]Zr). The broadening of the spectral lines of all oxygen atoms with increasing dose is suggested to cause both by disordering of the crystalline phase and by an increase in the diversity of SRO structures in the amorphous fraction.

Dose dependences of Si2p and Zr3d binding energy

The dose dependence of the Si2p binding energy (see Fig. 7a) is typical of dose response. According to the fitting (see Table 3), the disordered state corresponds to E_b(Si2p) = 102.3 eV. The cross section of the disordering process for E_b(Si2p) is lower than that for FWHM(Si2p); the structural transformations of SRO in Si-O sublattice responsible for the Si2p level shift take place mainly at low and middle doses (up to ~ 0.33·10^{18} α-decays/g). Conversely, the Zr3d binding energy increases only in a narrow low dose range (samples R1, MT and Z1), after which it gradually decreases in the series of samples Z1-Z6 (see Fig. 7b). That is the structural transformations of SRO in Zr-O sublattice responsible for the Zr3d level shift take place in a wide range of doses (up to ~ 5.1·10^{18} α-decays/g).

The increase in E_b(Si2p) and decrease in E_b(Zr3d) in the Z1-Z6 series correspond to an associated increase in the effective positive atomic charge Q_{eff}(Si) and a decrease in Q_{eff}(Zr). A change in the effective charge of atoms to the opposite direction is characteristic of complex oxides when they are separated into simple oxides, according to the known empiric rule (Urusov1987; Barr 1991). Namely, in complex oxide, the ionicity of a chemical bond with a higher ionicity in the initial simple oxide (in this case Zr-O in ZrO_2) as well as the covalency of a chemical bond with a higher covalency in the initial oxide (in this case, Si-O in SiO_2) both should increase in the complex oxide. An increase in Q_{eff}(Zr) from 2.72e (in ZrO_2) to 2.93e (in $ZrSiO_4$) and a decrease in Q_{eff}(Si) from 2.57e (in SiO_2) to 2.51e (in $ZrSiO_4$) were found on the basis of our ab initio calculations (Votyakov et al. 2011) in accordance with this rule. The implementation of this rule for $ZrSiO_4$ and ZrO_2, SiO_2 simple oxides was shown experimentally by the XPS (Guittetet al. 2001).

In XPS of the radiation-damaged zircon, the measured E_b values represent a weighted average over the entire set of non-equivalent SRO fragments. One can conclude that, with an increase in the damage degree, structural fragments of pure oxides appear and develop in the ensemble of SRO structures, resulting in the observed shift of E_b(Si2p) and E_b(Zr3d) to the opposite directions. Such fragments can comprise partially polymerised tetrahedra Q_n, characteristic of silicates, and 7-coordinated atoms $^{[7]}$Zr, characteristic of ZrO_2. This conclusion is consistent with the IR data on the partial SiO_4 polymerization (Farnan 1999; Farnan and Salje, 2001) and EXAFS data on the decrease in Zr coordination (Farges and Calas 1991) in metamict zircon.

At high doses ($D_\alpha^{ed} > p_2$), the change in the coordination of Zr from 8 to 7 is consistent with the appearance of an additional third type of oxygen O (Si, $^{[7]}$Zr, $^{[7]}$Zr) with $E_b \sim 531.6$ eV.

At moderate doses (up to $p_1 < D_\alpha^{ed} < p_2$), another reason for the decrease in the binding energy of Zr3d can be taken unto account. A decrease in the Zr3d binding energy was observed previously for solid solutions—$(ZrO_2)_x(SiO_2)_{1-x}$ films—with increasing x in the SiO_2 rich area (at $x \sim 0.1$–0.3) due to the forming of a donor—acceptor bond between zirconium and the bridging oxygen of polymerised fragments Si-O-Si (Lucovsky 2006). According to ab initio calculation results presented in this work, the positive shift in Zr core level is caused by the effect of donor–acceptor pair bonds. Thus, the reason for the decrease of the Zr3d binding energy in radiation damaged zircon may be the appearance of Zr cations surrounded by one (or more) oxygen atoms of O (Si, Si, $^{[8]}$Zr) instead of O (Si, $^{[8]}$Zr, $^{[8]}$Zr).

At low doses ($D_\alpha^{ed} < p_1$) the simultaneous increase in the effective charge of the Si and Zr cations is obviously connected with the crystalline fraction, because the amorphous fraction is small. One can speculate that the average effective atomic charges grow due to charge separation between anions and cations during the ionisation of the crystalline matrix, which consumes up to 90% of the energy of alpha particles (Ewing et al. 2003). However, the exact cause of this phenomena is not clear.

Considering the presence of tensile-compressive stresses in the heterogeneous amorphous-crystalline structure of radiation-damaged zircon (Chakoumakos et al. 1987; Murakami et al. 1991; Salje et al. 1999; Ríos et al. 2000), the dose dependences of a binding energy E_b can be attributed as with changes in the coordination of anions and cations, as well as with the lengths of Si-O and Zr-O bonds variations. According to Batsanov (2000, 2001), the general tendency for changes to occur in the chemical bonding upon compression of the lattice in simple AB compounds consists in an increase in covalency due to the increased orbital overlapping. The change in bond ionicity depends on the compressibility ratios of cation A and anion B; an increase in ionicity can be observed at the initial stage of compression for compounds with "hard" cations and "soft" anions. In complex oxides, the situation becomes more complicated due to the mutual influence of atoms; here, the simulations of the electronic structure are advantageous. Ab initio calculations predict the difference $\delta = 0.041e$ in the effective atomic charge of $^{[8]}$Zr due to a 5% variation in the unit cell significantly lower than $\delta = 0.209e$ (Votyakov et al. 2011) due to the changes the coordination of $^{[8]}$Zr to $^{[7]}$Zr. Therefore, we suppose that the coordination effect (the number and type of the nearest oxygen atoms in the zirconium SRO) prevails over the size effect (the length of the Zr-O bond) in the dose dependence of E_b.

Thus, oppositely directed trends of the change in effective charges of silicon and zirconium atoms (samples Z1-Z6) indicate an appearance of structural fragments of pure oxides in the ensemble of SRO structures, as well as a change in the nearest environment and the electronic structure of oxygen atoms. Changes in the SRO structures in the Si–O and Zr-O sublattices are not concurrent. In the range of low and medium doses ($D_\alpha^{ed} < p_2$), a partial polymerization of SiO_4 tetrahedra takes place, which is consistent with an increase in the concentration of oxygen atoms O (Si, Si) and/or O (Si, Si, $^{[8]}$Zr). At higher doses ($D_\alpha^{ed} > p_2$), the signs of 7-coordinated atoms $^{[7]}$Zr, characteristic of ZrO2, are detected. The latter agrees with the appearance of an additional third type of oxygen O (Si, $^{[7]}$Zr, $^{[7]}$Zr).

VB spectra at the variation of radiation damage degree

VB spectra (Fig. 6) of R1 and MT samples agree well with the previously predicted features of the electronic structure of zircon (Rignanese et al. 2001; Shchapova et al. 2010): the width of the O2s subband is 1.8 eV; the width of the O2p

subband is 6.0 eV; the total width of the band of oxygen states ΔE = 18.1 eV. The Zr4p states form narrow peak in the depth of the valence band with an energy 6.5 eV higher than the maximum energy of the O2s subband. The upper part of the valence band is formed by O2p with the admixture of Si3s, 3p, O2s and Zr4d states.

A gradual decrease in the density of binding O2p states at ~ 8–11 eV and its growth at ~ 13 eV (see Fig. 6, inset), as well as the expansion of the O2s states into the high-energy region, are observed with the increasing of the dose. Earlier, similar effect of the O2p- and O2s-subbands broadening in the XPS spectra were shown in quartz with a frame structure (O2p band ~ 10 eV) as compared to olivine with isolated SiO_4 tetrahedra (O2p band ~ 7 eV wide) (Zakaznova-Herzog et al. 2005). In the series of radiation-damaged Z1-Z6 zircons, this effect can be considered a sign of partial polymerisation of silicon-oxygen tetrahedra. This is consistent with the calculated data on the width of the O2s and 2p valence bands in perfect zircon structure and in the polymerised zircon structure near oxygen divacancies (Votyakov et al. 2011). Thus, the VB spectra independently confirm the increase in the diversity of the SRO structures of the oxygen sublattice with the possible separation of the amorphous fraction of the complex oxide $ZrSiO_4$ into simple SiO_2 and ZrO_2 at the level of short-range order. We note that the kinetic energy of valence electrons (1446–1486 eV) is much higher than the kinetic energy of core level electrons, which results in the greatest escape depth of former as compared with latter. The agreement of the results obtained from deep-lying layers (VB spectra) with those from a shallow near-surface region (core level spectra) confirm the validity of the XPS data for the studing of bulk (near-surface) atomic and electronic structure.

Transformation of silicon- and zirconium-oxygen sublattices

The effect of radiation damage on the electronic structure of silicon-oxygen and zirconium-oxygen sublattices in $ZrSiO_4$ is analysed using the Δ1 and Δ2 parameters, respectively (Fig. 9a):

$$\Delta 1 = E_b(O1s) - E_b(Si2p)$$

$$\Delta 2 = E_b(O1s) - E_b\left(Zr3d_{5/2}\right)$$

where $E_b(O1s)$ values are taken as a maxima obtained by fitting the O1s spectra by one general Voigt contour (see Table 2). The advantage of Δ1 and Δ2 is their independence from any arbitrary factors (in particular, the calibration of the energy scale). For clarity, the parameters δ1 and δ2 (Fig. 9a) characterising the distinction of the electronic structure of silicon-oxygen sublattice in $ZrSiO_4$ and SiO_2 (δ1) and zirconium-oxygen sublattice in $ZrSiO_4$ and ZrO_2 (δ2) are utilized:

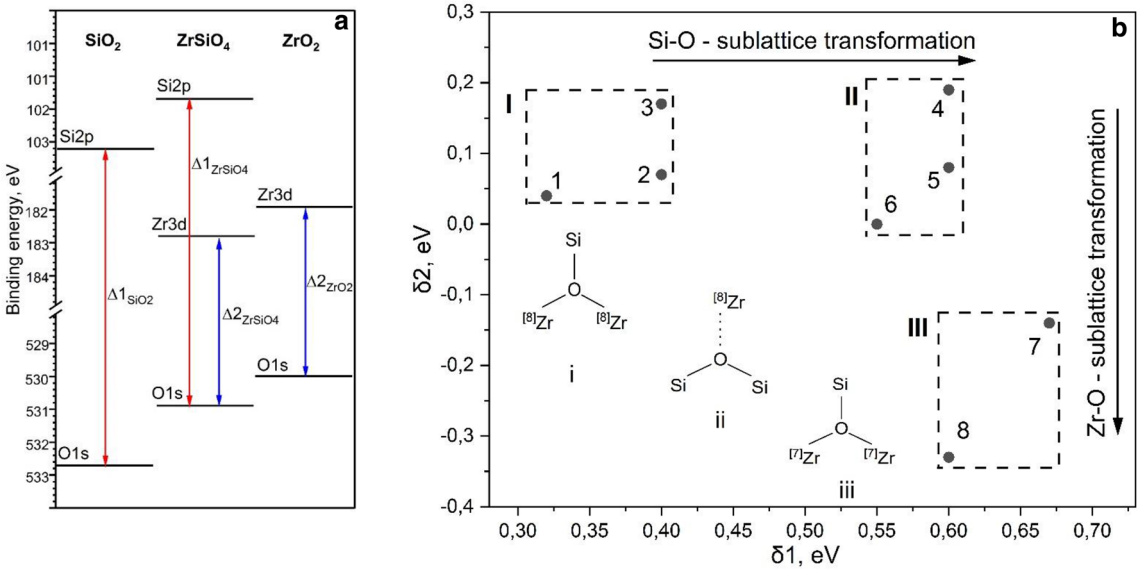

Fig. 9 Graphic illustration of the parameters Δ1, Δ2 (**a**), and the diagram δ1 vs. δ2 (filled circles) for samples R1 (1), MT (2), Z1 (3), Z2 (4), Z3 (5), Z4 (6), Z5(7) and Z6 (8). In Fig. a, the core level energies in $ZrSiO_4$ are given for sample R1, in SiO_2 and ZrO_2—for synthetic samples according to [Guittet et al. 2001]. In Fig. b, the dotted rectangles indicate the groups of samples with radiation damage doses D_α^{ed}: I—$0 \div 0.19 \cdot 10^{18}$ α-decays/g, II—$0.33 \div 1.22 \cdot 10^{18}$ α-decays/g, II—$3.4 \div 5.1 \cdot 10^{18}$ α-decays/g. The supposed sequence of the appearance and the increase in concentration of oxygen SRO structures in radiation-damaged zircon is schematically shown (i–iii). The arrows represent directions of changes in the electronic structure of the silicon- and zirconium-oxygen sublattices with increasing radiation dose

$$\delta 1 = \Delta 1\left(SiO_2\right) - \Delta 1\left(ZrSiO_4\right)$$

$$\delta 2 = \Delta 2\left(ZrO_2\right) - \Delta 2\left(ZrSiO_4\right)$$

where $\Delta 1(SiO_2) = 429.55$, $\Delta 2(ZrO_2) = 348.10$ eV according to (Guittet et al. 2001).

In the diagram δ1 vs. δ2 (Fig. 9b) three groups of samples are clearly identified: I—$\delta 1 = 0.30 \div 0.40$, $\delta 2 = 0.04 \div 0.17$; II—$\delta 1 = 0.55 \div 0.60$, $\delta 2 = 0.00 \div 0.19$; III—$\delta 1 = 0.60 \div 0.67$, $\delta 2 = (-0.33) \div (-\ 0.19)$. The groups correspond quite well to the percolation regions: I –crystalline sample R1, the samples MT and Z1 of low damage degree ($D_\alpha^{ed} < 0.2 \cdot 10^{18}$ α-decays/g, below p1); II –Z2-Z4 samples of medium and high damage degree ($0.3 \cdot 10^{18} < D_\alpha^{ed} < 1.2 \cdot 10^{18}$ α-decays/g, below and a little above p1); III – samples of a very high damage degree Z5, Z6 ($3.3 \cdot 10^{18} < D_\alpha^{ed} < 5.1 \cdot 10^{18}$ α-decays/g, above p_2). Upon transition from region I to II, there is a sharp increase in δ1 with a small change of δ2, i.e., a significant change in the electronic structure of the Si–O sublattice with a small change in the electronic structure of the Zr–O sublattice. This result is consistent with the partial polymerisation of SiO_4 tetrahedra at this stage (see Sect. 3.2, 3.3). In view of the small change in the electronic structure of the Zr-O sublattice, there is no reason to assume disturbance of its SRO at this stage; that means, the O (Si, Si) and O (Si, Si, $^{[8]}$Zr) fragments most likely occur without a change in the coordination number of Zr atoms. The main difference between the samples from groups II and III consists in a sharp decrease in δ1 with a small change of δ2, i.e., in a significant change in the electronic structure of Zr-O- with a less pronounced change in the Si-O-sublattice. Thus, this stage is most likely associated with a decrease in the prevailing coordination number of zirconium atoms from 8 to 7. A less significant, gradual decrease in δ2 within the groups II and III should be attributed to a gradual increase in concentration of fragments O (Si, Si, $^{[7,8]}$Zr) in these areas.

Thus, the sequence of transformations of the atomic and electronic structure of the Si-O and Zr-O sublattices is revealed. Evolution of the electronic structure of zircon with increasing radiation dose D_α^{ed} indicates: (1) partial polymerisation of the SiO_4 tetrahedra with the appearance of fragments O (Si, Si) and/or O (Si, Si, $^{[8]}$Zr) without changing the coordination number of Zr atoms in the dose range from $D_\alpha^{ed} \sim 0$ (R1 sample) to $D_\alpha^{ed} \sim p_1$ (and somewhat higher than this value, Z4 sample); (2) a decrease in the prevailing coordination number of zirconium atoms from 8 to 7 and a gradual increase in the concentration of fragments O (Si, Si, $^{[7,8]}$Zr) with a further dose increasing to values $D_\alpha^{ed} > p_2$ (Z5, Z6 samples).

Implications

This study has an important implications in understanding the type and the sequence of radiation-induced transformations of SRO structure and electronic state spectrum in zircon and, possibly, in other silicates.

First, an unequal response to radiation of two sublattices with different type of chemical bonding has been experimentally demonstrated. The structure of a more covalent sublattice (in this case, Si-O) exhibits less resistance to amorphization compared to the structure of a more ionic sublattice (in this case, Zr-O). Earlier in the literature, it was shown that the increase (decrease) of the short-range covalent component in material's total force field decreases (increases) its resistance (Trachenko et al. 2005); according to our studies, this turns out to be true for individual sublattices in $ZrSiO_4$.

Second, the information obtained on the structure and on the sequence of radiation-induced transformations of SRO may provide hints for the interpretation of some dose-dependent properties of zircon. In particular, this may concern the nature of intrinsic optical absorption and luminescence centers, for example, the yellow luminescence centers, which nature is ambiguous for decades (Krasnobayev et al. 1988; Nasdala et al. 2003; Kempe et al. 2010, 2016; Votyakov et al. 2011). However, we note that only averaged short-range order parameters have been obtained by XPS, while the details of the structure of individual areas (for example, the crystallite-amorphous interfaces) remained outside the scope of this work.

Third, the high-resolution XPS method with an effective surface charge neutralization has a great potential for the study of angstrom (at the short-range order level) perturbations of the composition and structure in near-surface layers of minerals. Such information seems to be useful in the analysis of radiation resistance, stability of solid solutions, and structural transformations due to external P, T-effects on minerals.

Conclusions

Core-level and valence-band X-ray photoelectron spectroscopy was employed to study the dose-dependent radiation effects in the short-range order and the electronic structure of natural U, Th-bearing zircon near-surface layers. A series of single crystals from secondary deposits of alkaline basalt rocks (Ratanakiri, Cambodia), carbonatites (Mud Tank, Australia) and placer deposits (Highlands, Sri Lanka) exhibiting wide variations in the accumulated radiation dose ($D \approx (0 \div 9.2) \cdot 10^{18}$ α-decays/g) was investigated. The dose values obtained using electron probe microanalysis and Raman micro-spectroscopy were used to correlate the samples with the two percolation transitions (p_1, p_2) in

the amorphous-crystalline structure of radiation-damaged zircon. For highly crystalline zircon ($D << p_1$), the binding energy and the linewidth values of the core levels O1s, Si2p, and $Zr3d_{5/2}$ were found $E_b = 530.9$, 101.7, 182.8 eV and FWHM = 1.32, 1.47, 1.16 eV, respectively, with the contribution of Si–OH surface states not exceeding 10%. The dose-dependent variations in E_b (up to 531.3, 102.4, 183.3 eV) and FWHM (up to 2.57, 1.77, 1.55 eV) were attributed to changes in the ensemble of non-equivalent short-range order structures. An increase in the dose resulted in the complication of the oxygen sublattice, with the following nearest environments of O atoms being distinguished: (1) the 3-coordinated atoms O (Si, $^{[8]}$Zr, $^{[8]}$Zr) with $E_b = 530.8$–531.2 eV in the amount of > ~3.5 apfu at $D < p_1$, characteristic of crystalline zircon; (2) the atoms O (Si, Si) and/or O (Si, Si, $^{[8]}$Zr) with $E_b = 532.6$ eV in the amount of ~ 0.5 ÷ 0.8 apfu at $p_1 < D < p_2$, characteristic of partially polymerized SiO_4 tetrahedra; (3) the atoms O (Si, $^{[7]}$Zr, $^{[7]}$Zr), $E_b = 531.6$ eV, well-determined in heavily-damaged zircons at $D > p_2$ (when the 3-coordinated atoms O (Si, $^{[8]}$Zr, $^{[8]}$Zr) amount is of ~ 1.7 apfu). For the first time, under an increase in the radiation dose, the oppositely directed changes in the effective charges of Si and Zr cations were detected in damaged zircon. This phenomenon was assigned to a dose-dependent increase in the content of the short-range order fragments characteristic of pure oxides SiO_2 and ZrO_2, as well as to the influence of the anions O (Si, Si, $^{[8]}$Zr). The broadening of the spectral lines of all atoms under an increase in the radiation dose was attributed to both the disordering of the crystalline phase and the increase in the diversity of short-range order structures in the amorphous fraction. In the valence band, a growth in the density of deep bonding O2p-states at ~ 13 eV and a shift of Zr4p level were established, which served as an independent confirmation of the dose-dependent partial SiO_4-polymerization and an increase in the effective charge of Zr. The sequence of transformations in the Si–O and Zr-O sublattices was not concurrent: a partial polymerization of SiO_4 tetrahedra occurs mainly at low and medium doses ($D < p_2$) both in the crystalline and amorphous fractions, while the 7-coordinated atoms $^{[7]}$Zr are mainly observed at higher doses ($D > p_2$) in the amorphous fraction. This study has an important implications in understanding the type and sequence of radiation-induced transformations of SRO structure and electronic state spectrum in zircon and, possibly, in other silicates.

Acknowledgements This work was supported by the Russian Foundation for Basic Research (RFBR), project 18-05-01153. Electron probe microanalysis was supported by the Russian Science Foundation (RSF), project 16-17-10283-P. The authors are grateful to Prof. L.Nasdala for providing the Ratanakiri zircon sample for research. We would like to thank Thomas A. Beavitt and Natalia G. Popova for their linguistic support.

Author contributions Conceptualization: Yu.V.S; Methodology: D.A.Z, I.S.Z, A.I.K, S.O.C; Formal analysis and investigation: I.S.Z, A.I.K, D.A.Z, Yu.V.S; Writing—original draft preparation: Yu.V.S; Writing—review and editing: D.A.Z, S.L.V, Yu.V.S, I.S.Z, A.I.K; Funding acquisition: Yu.V.S, S.L.V; Resources: S.O.C.

Funding The work was supported by the Russian Foundation for Basic Research, project 18-05-01153. Electron probe microanalysis was supported by the Russian Science Foundation, project 16-17-10283-P.

Data availability Experimental data are available from the authors in the form of numerical and graphic files; it can be provided upon request.

Compliance with ethical standards

Conflicts of interest The authors declare that they have no conflict of interest.

References

Balan E, Neuville DR, Trocellier P, Fritsch E, Muller J-P, Calas G (2001) Metamictization and chemical durability of detrital zircon. Am Mineral 86:1025–1033. https://doi.org/10.2138/am-2001-8-909

Balan E, Trocellier P, Jupille J, Fritsch E, Muller J-P, Calas G (2001) Surface chemistry of weathered zircons. Chem Geol 18:13–22. https://doi.org/10.1016/S0009-2541(01)00271-6

Bancroft GM, Nesbitt HW, Ho R, Shaw DM, Tse JS, Biesinger MC (2009) Toward a comprehensive understanding of solid-state core-level XPS linewidths: experimental and theoretical studies on the Si 2p and O 1s linewidths in silicates. Phys Rev B 80:075405. https://doi.org/10.1103/PhysRevB.80.075405

Barinsky RL, Kulikova IM (1977) Metamict transformation in some niobates and zircons according to X-ray absorption spectra. Phys Chem Miner 1:325–333. https://doi.org/10.1007/BF00308843

Barr TL (1991) Recent advances in X-ray photoelectron spectroscopy studies of oxides. J Vac Sci Technol A 9:1793–1805. https://doi.org/10.1116/1.577464

Batsanov SS (2000) Structural chemistry (facts and dependencies). Moscow Dialogue-MSU 2000: 291 P. ISBN 5-89209-597-5 (**in Russian**)

Batsanov SS (2001) Development of pauling's concepts of geometric characteristics of atoms. Crystallogr Rep 46(6):891–897. https://doi.org/10.1134/1.1420814

Begg BD, Hess NJ, Weber WJ, Conradson SD, Scheiger MJ, Ewing RC (2000) XAS and XRD study of annealed ^{238}Pu- and ^{239}Pu-substituted zircons ($Zr_{0.92}Pu_{0.08}SiO_4$). J Nucl Mater 278:121–224. https://doi.org/10.1016/S0022-3115(99)00256-1

Black LP, Gulson BL (1978) The age of the mud tank carbonatite, strangways range, northern territory. BMR J Aust Geol Geophys 3:227–232

Chakoumakos BC, Murakami T, Lumpkin GR, Ewing RC (1987) Alpha-decay-induced fracturing in zircon: the transition from the crystalline to the metamict state. Science 236:1556–1559. https://doi.org/10.1126/science.236.4808.1556

Chambers SA, Ohsawa T, Wang CM, Lyubinetsky I, Jaffe JE (2009) Band offsets at the epitaxial anatase $TiO_{2/n}$-$SrTiO_3$(001) interface. Surf Sci 603:771–780. https://doi.org/10.1063/1.1625113

Chanturia VA, Bunin IZ, Ryazantseva MV, Chanturia EL, Khabarova IA, Koporulina EV, Anashkina NE (2017) Modification of structural, chemical and process properties of rare metal minerals

under treatment by high-voltage nanosecond pulses. J Min Sci 53:718–733. https://doi.org/10.1134/S1062739117042704

Du J, Davanathan R, René CL, Weber WJ (2012) First-principles calculations of the electronic structure, phase transition and properties of ZrSiO4 polymorphs. Comput Theor Chem 987:62–70. https://doi.org/10.1016/j.comptc.2011.03.033

Duval Y, Mielczarski JA, Pokrovsky OS, Mielczarski E, Ehrhardt JJ (2002) Evidence of the existence of three types of species at the quartz-aqueous solution interface at pH 0–10: surface group quantification and surface complexation modeling. J Phys Chem B 202:2937–2945. https://doi.org/10.1021/jp012818s

Ewing RC (2007) Displaced by radiation. Nature 445:161–162. https://doi.org/10.1038/445161a

Ewing RC, Lutze W, Weber WJ (1995) Zircon: a host-phase for the disposal of weapons plutonium. J Mater Res 10:243–246. https://doi.org/10.1557/JMR.1995.0243

Ewing RC, Meldrum A, Wang L, Weber WJ, Corrales LR (2003) Radiation effects in zircon. In: Hanchar JM, Hoskin PWO (eds) Zircon, reviews in mineralogy and geochemistry, V53. Mineralogical society of America, Washington, pp 387–425

Fadley CS (2010) X-ray photoelectron spectroscopy: Progress and perspectives. J Electron Spectros Relat Phenomena 178–179:2–32. https://doi.org/10.1016/j.elspec.2010.01.006

Farges F (1994) The structure of metamict zircon: a temperature-dependent EXAFS study. Phys Chem Miner 20:504–514. https://doi.org/10.1007/BF00203221

Farges F, Calas G (1991) Structural analysis of radiation damage in zircon and thorite: an X-ray absorption spectroscopic study. Am Mineral 76:60–73

Farnan I (1999) ^{29}Si NMR characterization of the crystalline-amorphous transition in $ZrSiO_4$. Phase Transit 69:47–60. https://doi.org/10.1080/01411599908208007

Farnan I, Salje EKH (2001) The degree and nature of radiation damage in zircon observed by ^{29}Si nuclear magnetic resonance. J Appl Phys 89:2084–2090. https://doi.org/10.1063/1.1343523

Farnan I, Cho H, Weber WJ (2007) Quantification of actinide α-radiation damage in minerals and ceramics. Nature 445:190–193. https://doi.org/10.1038/nature05425

Finch RJ, Hanchar JM (2003) Structure and chemistry of zircon and zircon-group minerals. In: Hanchar JM, Hoskin PWO (eds) Zircon, reviews in mineralogy and geochemistry, V53. Mineralogical society of America, Washington, pp 1–25

Geisler T, Pidgeon RT, von Bronswijk W, Pleysier R (2001) Kinetics of thermal recovery and recrystallization of partially metamict zircon: a Raman spectroscopic study. Eur J Mineral 13:1163–1176. https://doi.org/10.1127/0935-1221/2001/0013-1163

Geisler T, Trachenko K, Rios S, Dove MT, Salje EKH (2003) Impact of self-irradiation damage on the aqueous durability of zircon ($ZrSiO_4$): implications for its suitability as a nuclear waste form. J Phys Condens Matter 15:L597–L605. https://doi.org/10.1088/0953-8984/15/37/L07

Ginster U, Reiners PW, Nasdala L, Chutimun Chanmuang N (2019) Annealing kinetics of radiation damage in zircon. Geochim Cosmochim Acta 249:225–246. https://doi.org/10.1016/j.gca.2019.01.033

Greczynski G, Hultman L (2018) Reliable determination of chemical state in x-ray photoelectron spectroscopy based on sample-work-function referencing to adventitious carbon: resolving the myth of apparent constant binding energy of the C 1s peak. Appl Surf Sci 451:99–103. https://doi.org/10.1016/j.apsusc.2018.04.226

Guittet MJ, Crocombette JP, Gautier-Soyer M (2001) Bonding and XPS chemical shifts in $ZrSiO_4$ versus SiO_2 and ZrO_2: charge transfer and electrostatic effects. Phys Rev B 63:125117. https://doi.org/10.1103/PhysRevB.63.125117

Haensel T, Reinmöller M, Lorenz P, Beenken WJD, Krischok S, Ahmed SI-U (2012) Valence band structure of cellulose and lignin studied by XPS and DFT. Cellulose 19(3):1005–1011. https://doi.org/10.1007/s10570-012-9681-9

Hochella MF (1988) Auger electron and X-ray photoelectron spectroscopies. In: Calas G, Hawthorne FC (eds) Reviews in mineralogy and geochemistry, V18. Mineralogical society of America, Washington, pp 573–637

Hoskin PWO, Schaltegger U (2003) The composition of zircon and igneous and metemorphic petrogenesis. In: Hanchar JM, Hoskin PWO (eds) Zircon, reviews in mineralogy and geochemistry, V53. Mineralogical society of America, Washington, pp 27–62

Iacona F, Kelly R, Marletta G (1999) X-ray photoelectron spectroscopy study of bombardment-induced compositional changes in ZrO_2, SiO_2, and $ZrSiO_4$. J Vac Sci Technol A 17:2771–2778. https://doi.org/10.1116/1.581943

Kempe U, Thomas SM, Geipel G, Thomas R, Plötze M, Böttcher R, Grambole G, Hoentsch J, Trinkler M (2010) Optical absorption, luminescence, and electron paramagnetic resonance (EPR) spectroscopy of crystalline to metamict zircon: evidence for formation of uranyl, manganese, and other optically active centers. Am Mineral 95:335–347. https://doi.org/10.2138/am.2010.3248

Kempe U, Trinkler M, Pöppl A, Himcinschi C (2016) Coloration of natural zircon. Can Mineral 54:635–660. https://doi.org/10.3749/canmin.1500093

Krasnobayev AA, Votyakov SL, Krokhalev VYa (1988) Spectroscopy of zircons. Nauka, Moscow ((**in Russian**))

Lucovsky G (2006) Electronic structure and chemical bonding in high-K transition metal and lanthanide series rare earth alternative gate dielectrics: applications to direct tunneling and defects at dielectric interfaces. In: Demkov AA, Navrotsky A (eds) Materials fundamentals of gate dielectrics. Springer Science and Business Media 109–178

Moulder JF, Stickle WF, Sobol PE, Bomben KD (1992) Handbook of X-ray photoelectron spectroscopy. Perkin-Elmer Corp, Eden, Prairie, MN, US

Murakami T, Chakoumakos BC, Ewing RC, Lumpkin GR, Weber WJ (1991) Alpha-decay event damage in zircon. Am Mineral 76:1510–1532

Nasdala L, Wolf D, Irmer G (1995) The degree of metamictization in zircon: a Raman spectroscopic study. Eur J Mineral 7:471–478. https://doi.org/10.1127/ejm/7/3/0471

Nasdala L, Pidgeon RT, Wolf D (1996) Heterogeneous metamictization of zircon on a microscale. Geochim Cosmochim Acta 60:1091–1097. https://doi.org/10.1016/0016-7037(95)00454-8

Nasdala L, Wenzel M, Vavra G, Irmer G, Wenzel T, Kober B (2001) Metamictization of natural zircon accumulation versus thermal annealing of radioactivity-induced damage. Contrib to Mineral Petrol 141:125–144. https://doi.org/10.1007/s004100000235

Nasdala L, Zhang M, Kempe U, Panczer G, Gaft M, Andrut M, Plotze M (2003) Spectroscopic methods applied to zircon. In: Hanchar JM, Hoskin PWO (eds) Zircon, reviews in mineralogy and geochemistry, V53. Mineralogical society of America, Washington, pp 427–467

Nasdala L, Reiners PW, Garver JI, Kennedy AK, Stern RA, Balan E, Wirth R (2004) Incomplete retention of radiation damage in zircon from Sri Lanka. Am Mineral 89:219–231. https://doi.org/10.2138/am-2004-0126

Nefedov VI, Vovna VI (1987) Electronic structure of chemical compounds. Nauka, Moscow ((**in Russian**))

Nesbitt HW, Bancroft GM (2014) High resolution core- and valence-level XPS studies of the properties (structural, chemical and bonding) of silicate minerals and glasses. In: Henderson GS, Neuville DR, Downs RT (eds) Spectroscopic methods in mineralogy and materals sciences, reviews in mineralogy and geochemistry, vol 78. Mineralogical society of America, Washington, pp 271–329

Palenik CS, Nasdala L, Ewing RC (2003) Radiation damage in zircon. Am Mineral 88:770–781. https://doi.org/10.2138/am-2003-5-606

Pidgeon RT, Nasdala L, Todt W (1998) Determination of radiation damage ages on parts of zircon grains by Raman microprobe: implications for annealing history and U-Pb stability. Mineral Mag 62A:1174–1175. https://doi.org/10.1180/minmag.1998.62A.2.280

Rignanese G-M, Gonze X, Pasquarello A (2001) First-principles study of structural, electronic, dynamical, and dielectric properties of zircon. Phys Rev B 63:104305. https://doi.org/10.1103/PhysRevB.63.104305

Rios S, Salje EKH, Zhang M, Ewing RC (2000) Amorphization in zircon: evidence for direct impact damage. J Phys Condens Matter 12:2401–2412. https://doi.org/10.1088/0953-8984/12/11/306

Salje EKH, Chrosch J, Ewing RC (1999) Is «metamictization» of zircon a phase transition? Amer Mineral 84:1107–1116. https://doi.org/10.2138/am-1999-7-813

Shchapova YuV, Votyakov SL, Kuznetsov MV, Ivanovsky AL (2010) Influence of radiation defects on electronic structure of zircon from X-ray photoelectronic spectroscopy data. J Struct Chem 4:687–692. https://doi.org/10.1007/s10947-010-0096-x

Shchapova YuV, Zamyatin DA, Votyakov SL, Zhidkov IS, Kukharenko AI, Cholakh SO (2020) Atomic and electronic structure of zircon according to high-resolution X-ray photoelectron spectroscopy: methodological aspects. In: Votyakov SL, Kiseleva DV, Grokhovskii VI, Shchapova YuV (eds) minerals: structure, properties, methods of investigation. Proceedings of the 10th all-Russian youth scientific conference. Springer Nature Switzerland AG https://doi.org/10.1007/978-3-030-49468-1_29

Siegbahn K (1974) Electron spectroscopy: an outlook. J Electron Spectros Relat Phenomena 5:3–97. https://doi.org/10.1016/0368-2048(74)85005-X

Trachenko KO, Dove MT, Salje EKH (2001) Atomistic modelling of radiation damage in zircon. J Phys Condens Matter 13:1947–1959. https://doi.org/10.1088/0953-8984/13/9/317

Trachenko K, Dove MT, Salje EKH (2003) Large swelling and percolation in irradiated zircon. J Phys Condens Matter 15:L1–L7. https://doi.org/10.1088/0953-8984/15/2/101

Trachenko K, Dove MT, Geisler T, Todorov I, Smith B (2004) Radiation damage effects and percolation theory. J Phys Condens Matter 16:S2623–S2627. https://doi.org/10.1088/0953-8984/16/27/002

Trachenko K, Pruneda JM, Artacho E, Dove MT (2005) How the nature of the chemical bond governs resistance to amorphization by radiation damage. Phys Rev B 71:184104. https://doi.org/10.1103/PhysRevB.71.184104

Urusov VS (1987) Theoritical crystal chemistry. MSU, Moscow ((**in Russian**))

Váczi T, Nasdala L (2017) Electron-beam-induced annealing of natural zircon: a Raman spectroscopic study. Phys Chem Miner 44:389–401. https://doi.org/10.1007/s00269-016-0866-x

Votyakov SL, Shchapova YuV, Khiller VV (2011) Crystal chemistry and physics of radiation and thermal effects in some U-Th-bearing minerals as the basis for the chemical microprobe age dating. Yekanerinburg, Publishing house of Ural Branch of RAS 330 ISBN 978-594332-091-0 (in Russian)

Weber WJ, Ewing RC, Wang LM (1994) The radiation-induced crystalline-to-amorphous transition in zircon. J Mater Research 9:688–698. https://doi.org/10.1557/JMR.1994.0688

Wopenka B, Jolliff BL, Zinner E, Kremser DT (1996) Trace element zoning and incipient metamictization in a lunar zircon: application of three microprobe techniques. Am Mineral 81:902–912. https://doi.org/10.1557/JMR.1994.0688

Zakaznova-Herzog VP, Nesbitt HW, Bancroft GM, Tse JS, Gao X, Skinner W (2005) High-resolution valence-band XPS spectra of the nonconductors quartz and olivine. Phys Rev B 72:205113. https://doi.org/10.1103/PhysRevB.72.205113

Zakaznova-Herzog VP, Nesbitt HW, Bancroft GM, Tse JS (2006) High resolution core and valence band XPS spectra of non-conductor pyroxenes. Surf Sci 600:3175–3186. https://doi.org/10.1016/j.susc.2006.06.012

Zakaznova-Herzog VP, Nesbitt HW, Bancroft GM, Tse JS (2008) Characterization of leached layers on olivine and pyroxenes using high-resolution XPS and density functional calculation. Geochim Cosmochim Acta 72:69–86. https://doi.org/10.1016/j.gca.2007.09.031

Zamyatin DA, Shchapova YuV, Votyakov SL, Nasdala L, Lenz C (2017) Alteration and chemical U-Th-total Pb dating of heterogeneous high-uranium zircon from a pegmatite from the Aduiskii massif, middle Urals, Russia. Mineral Petrol 111:1–23. https://doi.org/10.1007/s00710-017-0513-3

Zeug M, Nasdala L, Wanthanachaisaeng B, Balmer WA, Corfu F, Wildner M (2018) Blue Zircon from Ratanakiri, Cambodia. J Gemmol 36:112–132. https://doi.org/10.15506/JoG.2018.36.2.112

Zhang M, Salje EKH (2001) Infrared spectroscopic analysis of zircon: radiation damage and the metamict state. J Phys Condens Matter 13:3057–3071. https://doi.org/10.1088/0953-8984/13/13/317

Zhang M, Salje EKH, Ewing RC, Farnan I, Ríos S, Schlüter J, Leggo P (2000) α-decay damage and recrystallization in zircon: Evidence for an intermediate state from infrared spectroscopy. J Phys Condens Matter 12:5189–5199. https://doi.org/10.1088/0953-8984/12/24/310

Zhang M, Salje EKH, Farnan I, Graeme-Barber A, Daniel P, Ewing RC, Clark AM, Lennox H (2000) Metamictization of zircon: Raman spectroscopic study. J Phys Condens Matter 12:1915–1925. https://doi.org/10.1088/0953-8984/12/8/333